Ann. Geophys., 32, 401–420, 2014
www.ann-geophys.net/32/401/2014/
doi:10.5194/angeo-32-401-2014

Annales Geophysicae
Open Access

Wind patterns associated with the development of daytime thunderstorms over Istria

G. Poljak[1], M. T. Prtenjak[1], M. Kvakić[2], N. Strelec Mahović[3], and K. Babić[1]

[1]Department of Geophysics, Faculty of Science, University of Zagreb, Zagreb, Croatia
[2]CNRM-GAME, Meteo-France/CNRS URA 1357, Toulouse Cedex, France
[3]Meteorological and Hydrological Service, Zagreb, Croatia

Correspondence to: M. T. Prtenjak (telisman@gfz.hr)

Received: 9 November 2013 – Revised: 17 February 2014 – Accepted: 23 February 2014 – Published: 14 April 2014

Abstract. The northeastern (NE) Adriatic in the northern Mediterranean is the area with (i) the highest frequency of thunderstorms in Croatia, and (ii) frequent appearances of sea breeze (SB) along the coast. This study investigates the impact of the combined large-scale wind (associated with particular synoptic conditions) and the SB on the moist convection development over the NE Adriatic. The four selected cases were (i) chosen on the basis of a daytime moist convection; (ii) supplemented by one of the dominant large-scale winds with seaward (NE, NW) and landward (SW, SE) directions and (iii) simulated by WRF numerical model.

The near-surface wind patterns consisted of SBs along the coastline, generated a narrow eastward-moving convergence zone (CZ) along the area if the large-scale wind was less than 9 m s^{-1} (below 500 hPa). Apart from the low-level CZ, the advection of large-scale wind influenced the lifetime and movement of the initial Cb cells. While the local front collision with the NE wind advection caused the thunderstorm to propagate southward, the CZ and fronts interaction determined the afternoon northwestward storm movement against the NW large-scale wind. Due to particular synoptic background, the thunderstorm event in SE case was the shortest with only a minor impact on the SB. While the origins and locations of storm cells were completely controlled by the low-level CZ and the upward advection of low-level moisture at the SB front, the most typical convective case with SW warm-wet wind only partially supported the SB–Cb interaction.

Keywords. Meteorology and atmospheric dynamics (convective processes; mesoscale meteorology; precipitation)

1 Introduction

The initiation and evolution of deep convection highly depends on topography and both the synoptic and mesoscale conditions (e.g. Cotton et al., 2011; Wang et al., 2013). If the synoptic forcing is weak, the development of local circulations dominates, for example, sea/land breeze (SB/LB), slope winds and valley winds. Then, the interaction between the local fronts could easily be a cause of deep convection (e.g. Pozo et al., 2006; Qian, 2008) if they are supported by the favourable mid-tropospheric conditions (e.g. Barthlott et al., 2006; van Zomeren and van Delden, 2007; Sow et al., 2011). The convection is often observed during the collision of two SB fronts (e.g. Nicholls et al., 1991; Crook, 2001) or the gust front and an SB front (e.g. Wilson and Megenhardt, 1997) when the merging of the fronts affects the intensity of thunderstorms and the amount of convective precipitation. For example, studying Hectors over the Tiwi Islands near the northern Australian coast, Carbone et al. (2000) and Crook (2001) reported the dominance of the interaction of gust fronts and an SB front in 80 % of all recorded cases. Only 20 % of the observed thunderstorms were initiated by the collision of the SB fronts coming from the south and the north coast of the island. Numerical experiments by Saito et al. (2001) showed that topography characteristics such as height and surface area of the island determined the merger time of the clouds and the intensity of convection. Some studies revealed that storms could occasionally form on horizontal convective rolls (Kingsmill, 1995; Fovell, 2005). They interact with the SB front simultaneously causing thermally induced gravity waves that can favour or suppress the formation of new convection (Stechmann and Majda, 2009). Because of the wind

shear, one side of the pre-existing convection can be more favourable for the formation of new convection cells or systems than the other side.

The principal characteristics of the gust front (e.g. Wakimoto, 1982; Cotton et al., 2011) and SB front (e.g. Kingsmill, 1995; Prtenjak et al., 2006; Miao et al., 2009) are very similar because they both belong to gravity currents (Simpson, 1997). Identified by large updraughts, the gust or SB front bounds the current that consists of a body of high-density (and cold) air. The other main features are a nose of the current, an elevated head and a turbulent wake behind the head. Although both fronts have similar heights within the boundary layer ranging from 0.5 to 2 km, they differ in intensity, speed and lifetime. Unlike the upward vertical velocities within the SB front, where they can be up to $2\,\mathrm{m\,s^{-1}}$, the updraughts within gust fronts are stronger and can reach $20\ \mathrm{m\ s^{-1}}$ (Cotton et al., 2011). The life span of a SB front is associated with the diurnal heating cycle of the atmosphere (i.e. ~ 10 h), while the gust front is a much shorter lived phenomenon linked with the lifetime of cumulonimbus (Cb), which can survive for just less than 1 h.

Many years of intensive research on the impact of SB occurrences on single-cell and multi-cell thunderstorms have been performed in Florida. The location and longevity of thunderstorms as well as the total amount of precipitation were controlled by the areal extent, magnitude and depth of the low-level convergence (Wilson and Megenhardt, 1997; Shepherd et al., 2001) caused by the SBs. The convergence appeared approximately 90 min before the detection of convective clouds on radar images (Ulanski and Garstang, 1978). Usually, a narrow zone of very high convective available potential energy (CAPE) occurred due to enhanced turbulent heat fluxes, and convection began within a few kilometres between the two SB fronts causing moisture advection upward (Nicholls et al., 1991). Above the two SB fronts, intense convective cells near the centre of convergence also developed. It was noted that while one cell usually died, the other became stronger and could start 1 or 2 new cells. Secondary cell development and rainfall production were highly influenced by the 850–500 hPa moisture content (Shepherd et al., 2001). Typical orders of magnitudes of both updraughts and downdraughts in Florida's storms exceeded $10\,\mathrm{m\,s^{-1}}$ (Yuter and Houze Jr., 1995).

In Europe, the Mediterranean is one of the most active convective areas (e.g. Christian et al., 2003), and a variety of observational (e.g. van Delden, 2001; Manzato, 2007; Strelec Mahović and Zeiner, 2009; Azorin-Molina et al., 2009) and modelling (e.g. Rakovec et al., 2004; Belušić et al., 2007; Belušić and Strelec Mahović, 2009; Mastrangelo et al., 2011; Barthlott and Kirshbaum, 2013) studies have been conducted to examine many individual convective events or their climatology. For example, Kolios and Feidas (2010) found that the formation of mesoscale convective systems was strongly correlated with orography, where convection initiation is favoured by thermal forcing over land and orographic lifting, but with some differences in size, duration and diurnal variations compared with those in the tropics or the USA. The preferred areas of convective systems were along the northern coasts of the Mediterranean basin with "hot spots" in the Gulf of Genoa and the Adriatic Sea. Recently, Mikuš et al. (2012) analysed the available lightning data above Croatia detecting 402 thunderstorm days in the warm parts of the 2006–2009 period. The study showed that the northeastern (NE) Adriatic (Fig. 1), particularly the Istrian peninsula, has the highest annual number of days with thunderstorms in Croatia. The results were very similar to those for the nearby Friuli Venezia Giulia plain squeezed between the Adriatic Sea and the Julian and Carnic Alps (Manzato, 2007; Manzato, 2012). The typical synoptic conditions were (i) low pressure formations that took up to 72 % out of a total 251 events for NE Adriatic, and (ii) almost non-gradient (NG) surface pressure field which accounted for 21 % of the total thunderstorm day number. On 82 % of all days with convective activity, three dominant wind regimes above the NE Adriatic were observed on a large scale: from the SW (46 %), NE (18 %) and NW (18 %) directions. Babić et al. (2012) analysed the relationship between Cb clouds and SB over the Istrian peninsula in the period of 1997–2006. The results have revealed that in at least 51 % of daytime Cb occurrences, SB develops along the coast. This geographical area regularly experiences SB on 50 % of all summer days on average according to the climatological studies (e.g. Prtenjak and Grisogono, 2007).

Bearing in mind that SB characteristics highly depend on location and local topographic characteristics, such as the size of the water surface, the height and slope of the coastal terrain and the curvature of the coastline (e.g. Miller et al., 2003; Crosman and Horel, 2010), our knowledge about the SB impact on the deep convection over the Mediterranean coast is still limited. A convex coastline and increased surface roughness over land can significantly contribute to the low-level (SB) convergence and therefore to the severe convection, lightning and coastal precipitation. Recently, Heiblum et al. (2011) and Mazón and Pino (2013) showed that low-level convergence of LB and synoptic winds close to the coastline as well as the frictional convergence and high mountainous ridges have significant effects on the formation of convection and precipitation. Still, most of the research conducted over the Mediterranean has been focused on the large, strong events enriched with high amounts of precipitation and, to a lesser extent, on the meso-γ-scale storms associated with SB/LB. Thus, the aim here is to investigate the influence of the combined large-scale wind and thermally generated winds on individual thunderstorms in one very convective area, the NE Adriatic.

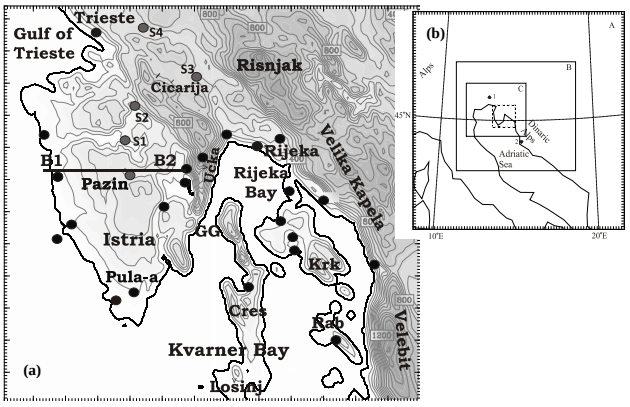

Fig. 1. (a) A close-up of the NE Adriatic (dotted rectangle in the upper right panel) with topography depicted by contours every 100 m (for geographical details see the text) between 0 and 1500 m. Circles represent the positions of measuring sites; hourly meteorological (Pazin, Pula-a and Rijeka) and climatological measurements. The thick solid black line denotes the base of vertical cross-section (B1B2) shown in later figures and Table 2. **(b)** The upper right panel indicates the coarse-grid (A), mid-frame (B) and fine-grid (C) WRF model domains, respectively. Numbered dot 1 denotes Udine (46.03° N, 13.18° E) radio sounding station and dot 2 correspond to the radio sounding station Zadar (44.10° N, 15.35° E).

2 Data and methodology

2.1 The area of research

The NE Adriatic area is located on the very northern edge of the central Mediterranean and consists of a very complex coastline, a large number of islands and a large peninsula, Istria (Fig. 1a). Surrounded by the shallow sea on three sides, Istria is characterised by three geographical regions. The mountainous region is characterised by the northern Trieste karst and Ćićarija (∼ 1100 m high) mountains that stretch toward the mountain of Učka to the east, which is the highest Istrian peak (1396 m a.g.l. - above ground level). The lower coastal region is in the west and south of the peninsula (where Pula airport is placed, see Pula-a in Fig. 1a), and the open low limestone plateau (where the Pazin station is located) is in the central part of the peninsula. Along the mainland shore, the mountain range continues with the mountains of Risnjak (∼ 1500 m), Velika Kapela (∼ 1600 m a.g.l.) and Velebit (∼ 1600 m a.g.l.). The larger islands within the Kvarner Bay are Krk, Cres, Mali Lošinj and Rab, which form a few narrow sea passages, such as the Great Gate (GG), between the islands of Cres and Istria. The islands of Krk and Cres, along with the mainland, surround the smaller Rijeka Bay.

2.2 Selected cases and used data

To obtain insight into the spatial and temporal distribution of SB and Cb interactions, we selected and simulated several periods chosen from the Babić et al. (2012) and Mikuš et al. (2012) data sets. For that purpose we used satellite images (NOAA 16–18 and Meteosat 7, 8), data about total lightning discharges from LINET network (Betz et al., 2009), radar data from Lisca radar station (ARSO – www.meteo.si), radio sounding data in Udine and Zadar (http://weather.uwyo.edu/) and near-surface measurements from a standard meteorological Croatian network (see positions in Fig. 1a).

The main criterion for selection was a daytime convection, that is, the existence of Cb cell(s) in satellite images and/or total lightning during the daytime hours (from 11:00 CET to 21:00 CET) over the NE Adriatic. Accordingly, the measured rainfall should occur only during the light part of a day. Only noon/afternoon occurrence of moist convection means also that SB could be generated along coastlines. A comprehensive inspection allows us to select the cases that contain an interaction of Cb and SB above Istria supplemented by one of the dominant large-scale wind types with seaward (NE, NW) and landward (SW, SE) directions over the NE Adriatic. The selected cases are in Table 1.

Although the convective/rainfall pattern never depends only on the large-scale wind pattern, Mikuš et al. (2012) have revealed the most typical weather type (i.e. general atmospheric conditions) that appears for each wind regime. The authors concluded that while the NE wind is usually generated by the northern side of the cyclones, the NW wind occurs along the rear side of the cyclone or upper-level trough. The position of these low pressure centre patterns is located eastward/northeastward from target area and determines whether it will be the advection of a cold(er) air above Croatia by NE or NW wind. On the contrary, the SW (quite frequent) and SE (less frequent) flows are usually created by a front side of a well-developed cyclone (or a trough) with the centre over the central Europe and the Central Mediterranean, respectively. These winds distribute warm and moisture-rich air over the NE Adriatic/Croatia. Therefore, a detailed analysis of selected periods and cases will provide an additional insight in relation to the general characteristics of the atmospheric conditions obtained by the climatological analysis in Mikuš et al. (2012).

2.3 Mesoscale model

The research mesoscale version of the non-hydrostatic Weather and Research Forecasting WRF-ARW model (Version 3.3; Skamarock et al., 2008) has been used for the simulation periods of 36 h (in cases C1–C3, Table 1) and 60 h (case C4) starting at noon of the previous day to reproduce chosen cases. The initial and boundary conditions were taken from the global ECMWF analysis and the lateral boundary conditions were updated every 6 h. The ECMWF analysis resolution was not constant: in the four case studies analysed here, it was T511 (0.351° horizontal resolution) before 1 February 2006, and T799 (0.225° horizontal resolution) after. The vegetation and land-use data come from the USGS 24 category data set at a resolution of 30″. Three domains

Table 1. Selected simulated WRF cases with the Cb clouds over Istria in which the SB interacts with one of the dominant types of large-scale (LS) wind (NE, NW, SE, SW). The second column displays the most dominant pressure pattern in general atmospheric conditions. Both the SB duration and wind speed (WS) were evaluated at the Pula airport site (tip of the Istria peninsula). The measured daily precipitation is for Pazin (see Fig. 1). Both onset and ending of the thunderstorms were determined on the basis of radar data.

Cases (date)	General atmospheric conditions	Dominant LS wind	Thunderstorm onset–end (CET)	SB duration onset–end (CET)	Max hourly 10 m WS ($m\,s^{-1}$)	Daily R (mm) onset–end (CET)
Case C1 9 Jul 2006	Rear northern side of cyclone over Black Sea with almost NG pressure field over Istria	NE	10:50–16:00	09:00–19:00	5.1	1.7 (13:00–14:00)
Case C2 8 Aug 2006	Rear southern side of cyclone over Pannonian Plain with relatively weak surface forcing above Istria	NW	11:10–16:30	09:00–13:00	4.1	0
Case C3 8 Jun 2003	Rear southern side of anticyclone over Balkan Peninsula	SE	12:40–16:30	09:00–20:00	3.6	9.1 (13:00–15:00)
Case C4 6 Jul 2009	Front southern side of cyclone over western/central Europe	SW	08:50–18:50	09:00–20:00	3.1	0.5 (11:00–13:00)
7 Jul 2009			00:00–07:10; 08:40–17:00	–	5.1	5.5 (00:00–24:00)

with a two-way nesting on a Lambert conformal projection were applied to reproduce the thermodynamic characteristics over the NE Adriatic. The horizontal resolutions of model domains were 13.5 km, 4.5 km and 1.5 km (Fig. 1b). The top of the atmosphere is set at 50 hPa. The vertical domain was divided by the 81 sigma levels, with the lowest half-sigma level at $\sim$ 12 m above the ground and with 13 levels in the lowermost 2 kilometres. The vertical resolution stretches from the lowest 25 m up to 250 m in the middle and upper parts of the troposphere. The WRF physics options were kept the same for all simulations and correspond to the Mellor–Yamada–Janjić scheme for the planetary boundary layer: a rapid radiative transfer model and a Dudhia scheme for long-wave and short-wave radiation, respectively; a Lin microphysics scheme with ice, snow and graupel processes; an Eta surface layer scheme based on Monin–Obukhov theory; and a five-layer thermal diffusion scheme for soil temperatures.

3 Results and discussion

In Fig. 2, 27 h backward trajectories for three neighbouring points (S1, S2, and Pazin in Fig. 1a) show four dominant large-scale wind directions and advection of the air above Istria; from the continent in cases C1 and C2 (see Table 1) and landward air advection from the Adriatic Sea in the cases C3 and C4, respectively. The trajectories were calculated by means of modelled wind fields at a fixed level of 500 hPa at the largest WRF model domain ($\Delta x = 13.5$ km). In general, consecutive parcel positions are relatively close, which, however, indicates the relatively low modelled wind speeds with some differences in their dynamics. Thus, while the NE advection of the air parcel for the case C1 suggests very low modelled wind speeds (in accordance with radio sounding data in Fig. 3b), in case C3, the SE wind flow is more uniform during the examined period. The other two cases are characterised by the stronger ambient wind with the opposite behaviour; the NW wind in case C2 is getting slower as the air approaches Istria and in case C4, the SW large-scale flow gradually accelerates toward peninsula.

3.1 Case with the NE large-scale wind (case C1)

In case C1 (9 July 2006), the NE Adriatic (together with the large portion of the European continent) was under the influence of an almost NG high-pressure field at the surface, with high pressure centres residing over NE Europe and the mid-Atlantic (Fig. 3a). The combination of a high pressure centre over NE Europe and a very weak low over the Black Sea led to a generally NE large-scale flow over the Adriatic area and Croatia in the lower troposphere. In the upper levels an interesting feature was a pronounced difluence over the Alpine region and further towards eastern Europe. According to the radio sounding at Zadar (see Fig. 1b) at 00:00 UTC, the NE flow with speeds less than $10\,m\,s^{-1}$ dominated in most of the troposphere (Fig. 3b). The convective potential is given by the indices of instability at Zadar and Udine; CAPE $> 600\,J\,kg^{-1}$ at both stations, and with

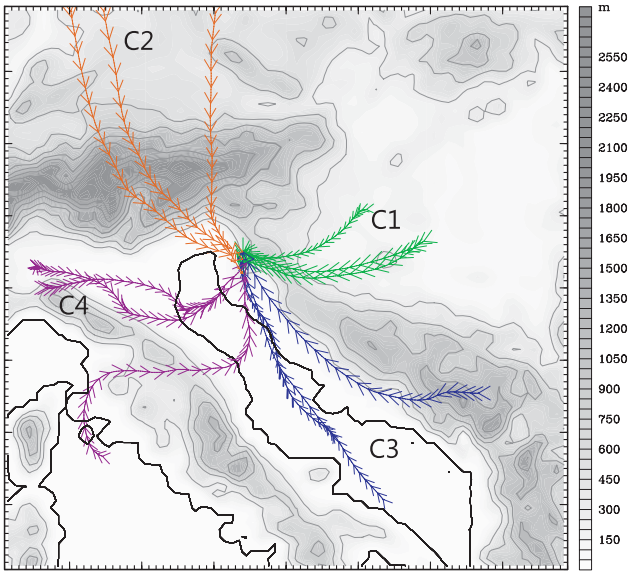

Fig. 2. Depicted are 27 h three-dimensional backward trajectories arriving at the three nearby points (grey dots Pazin, S1, S2 in Fig. 1a) in Istria at 16:00 CET for four examined cases: on 9 July 2006, (case C1; green), 8 August 2006 (case C2; orange), 8 June 2003 (case C3; blue) and 7 July 2009 (case C4; violet). The trajectories were calculated at 13.5 km horizontal resolution within the largest model domain at 500 hPa level and arrows represent parcel positions for every hour.

convective inhibition (CIN) of $\sim -150\,\mathrm{J\,kg^{-1}}$. Although the bulk Richardson number (BRN) is relatively small in Zadar (~ 38; Fig. 3b), it is large in Udine (> 1400) indicating little shear, strong buoyancy and possible multi-cell convective storms on this part of the Adriatic coast. Over the NE Adriatic, the daytime convective storm occurred with the lifetime of 5 h. The Istrian Cb clouds gave (i) a small amount of precipitation in Pazin (Table 1) and (ii) total lightning discharges that made a narrow strip of 60 km flashes (Fig. 3c) along the peninsula. Surface measurements reveal two characteristics: relatively long-lasting onshore flows along the Istrian coast (see Appendix A) and the convergence zone that looms in the middle of the peninsula (Fig. 3d).

In Fig. 4, the simulated composite reflectivity is accompanied by the near-surface wind field in the smallest model domain showing the SB and thunderstorm system (mesoscale) evolution over Istria. Apart from the modelled field, the radar images (ARSO – www.meteo.si) offer a qualitative comparison for this case regarding the development and movement of the thunderstorm. Additionally, the thermodynamic characteristics of the SB and convection are summarised quantitatively in Tables 2 and 3, respectively. Since the SB system can be described on several spatial scales (SB circulation, SB flow and SB front), the four widely used measures of the horizontal and vertical length scales and the horizontal and vertical wind speed scales (Crosman and Horel, 2010) were used here (shown in Table 2) to describe the SB intensity. The parameters related to SB characteristics are determined during 10:00–12:00 CET while they are still largely undisturbed.

The model generated convective activities directly above the mountainous ridge along the NE part of the peninsula (Fig. 4a). However, although the location was generally in good agreement with the corresponding observed data (Fig. 4e); the model showed a somewhat earlier development of the Cb cells (by 1 h). During the next hours, due to the dominance of the NE large-scale wind, both the modelled (Fig. 4b, c) and the observed radar echoes (Fig. 4f, g) form a long line along the peninsula corresponding to the total lightning discharges in Fig. 3c. The evolution of the convection is still slightly faster in the measurements compared to the model, and thus, it decays 1 h later than in the observations, after 16:00 CET (Fig. 4d, h).

Simultaneously, the near-surface wind data showed the formation of the SB flow, apparently starting at 08:00 CET and reaching a maximum about 13:00 CET (Figs. 4 and A1), which is in accordance with the measurements (in Fig. 3d). From 10:00 to 12:00 CET, the onshore SB flow and the corresponding SB front are located approximately 10–15 km inland of the western peninsula coast (Fig. 4). A large part of the peninsula is under the influence of the low-level NE to easterly wind (supported by the ambient NE wind) that forms a horizontal convergence zone with the shallow onshore NW to westerly flow. The effect of the opposite ambient wind here is a relatively slow penetration of the western SB inland. The SB is in a form that corresponds to the gravity current (e.g. Simpson, 1997) and has the maximum speed of the SB up to $5\,\mathrm{m\,s^{-1}}$ (Table 2), the height of the SB front to approximately 1800 m and the SB body (i.e. depth of onshore flows) up to 800 m (not shown). At the very narrow SB front, the largest updraughts among cases, reach approximately $1\,\mathrm{m\,s^{-1}}$ (in the range of 1–2 km a.g.l. Table 2) before colliding with the deep convection. Additionally, the slow inland penetration of the western SB front also coincides with the results of a recent study above the same geographical region where the SB development within a moderate bora wind environment was investigated (i.e. NE wind, Prtenjak et al., 2010).

The surface temperature difference between the interior of the peninsula and sea surface did not exceed 3 K (not shown), with a large temperature gradient (across the SB front) occurring at the narrow convergence zone. The same area can be easily recognised by the maximum CAPE ($\sim 2000\,\mathrm{J\,kg^{-1}}$) values, where the CAPE gathers due to the heat and moisture surface fluxes during the SB inland penetration close to the front (Fig. 5a). The same was found in Florida (e.g. Wilson and Megenhardt, 1997), where deep convection resulted from a significant low-level convergence within the thin convergence zone (up to 3 km wide in C-band radar images) that was followed by a large CAPE. The maximum CAPE values here correspond to a lower lifting condensation level (LCL ~ 1000 m, Table 3) and a lower level of free convection

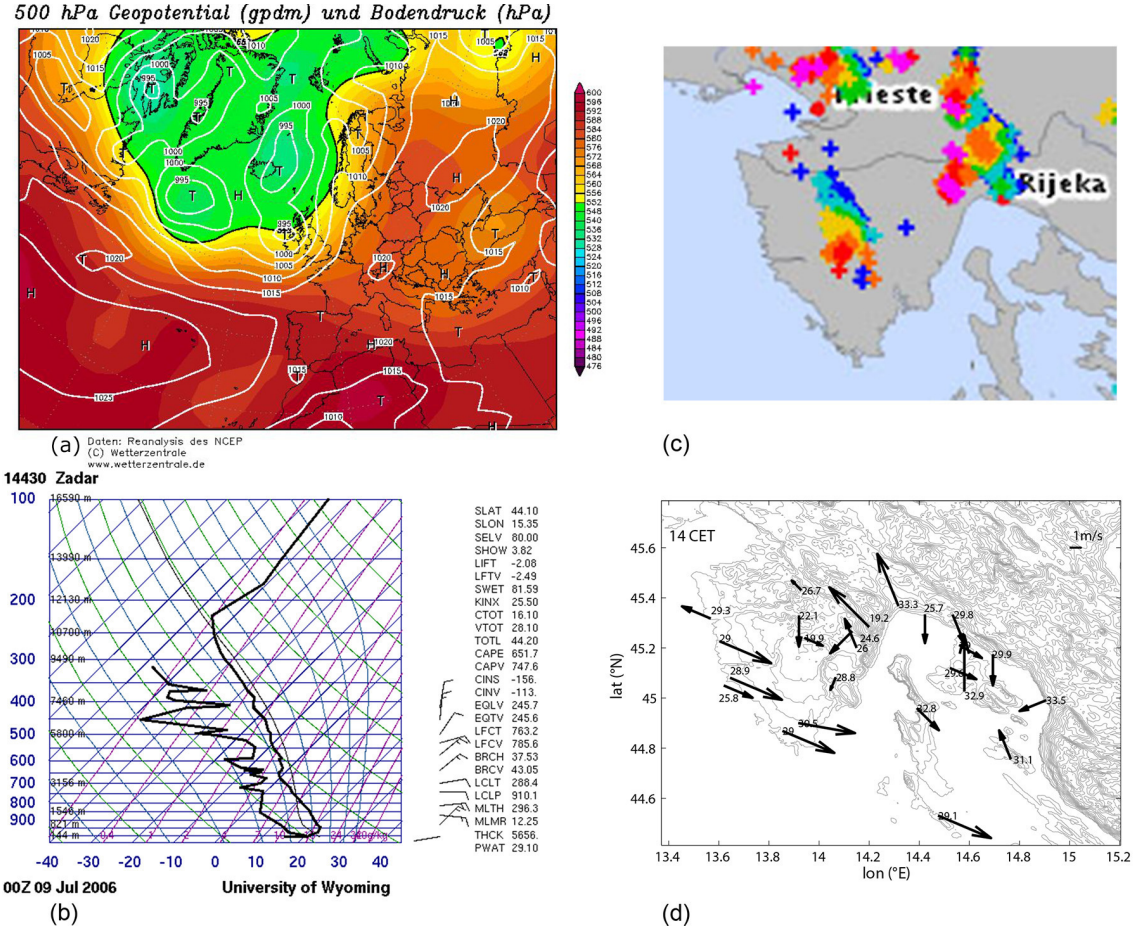

Fig. 3. Case C1, 9 July 2006: **(a)** surface pressure distribution (white lines) and geopotential of 500 hPa pressure level (filled areas) at 00:00 UTC (i.e. 01:00 CET) (source: http://www.wetterzentrale.de/topkarten/fsreaeur.html). **(b)** Radio sounding profiles plotted on a skew T-log p diagram in combination with convective indices in Zadar (44.10° N, 15.35° E) at 00:00 UTC (i.e. 01:00 CET); **(c)** lightning distribution from 13 to 14:00 CET from LINET network (Betz et al., 2009). The coloured crosses indicate the detection of lightning within one hour: purple (< 3 min), red (10–3 min), orange (20–10 min), yellow (30–20 min), green (40–30 min), light blue (50–40 min) and blue (> 50 min); **(d)** the measured 10 m wind vectors (m s^{-1}) and 2 m air temperatures (°C) at 14:00 CET (measuring sites in Fig. 1a).

Table 2. Sea breeze (SB) characteristics and thermodynamical variables from the model averaged in time (for period of 10:00–12:00 CET), over the Istria peninsula for four selected cases. Parameters were defined along the vertical cross-section (B1B2) shown in Fig. 1. In the table, abbreviations represent max SB speed = maximum wind speed in the western onshore flow usually between 200 and 300 m a.g.l, SBF: sea breeze front and low-level MFC: moisture flux convergence (e.g. Eq. 5 in Banacos and Schultz, 2005). Inland penetration of the SB and SBF height are determined by the position of the SBF updraft. A negative divergence ($\partial u/\partial x + \partial v/\partial y < 0$) in the table means maximum horizontal convergence value associated with SBF.

Parameters in vertical cross section (10:00–12:00 CET)	Case C1 9 Jul 2006	Case C2 8 Aug 2006	Case C3 8 Jun 2003	Case C4 6 Jul 2009
max SB speed (m s^{-1})	4.1	5.0	3.8	5.0
SB inland penetration (km) at 11:00 CET	11	13.5	15	14.7
SBF height (m)	1800	1266	1400	1200
SBF updraft (cm s^{-1})	93	50	73	62
Divergence $\times 10^{-3}$ (s^{-1}) across SBF	−1.3	−0.8	−0.8	−1.0
low-level q in SB (g kg^{-1})	13.1	12.8	15.1	14.3
MFC at SBF $\times 10^{-3}$ (g kg^{-1} s^{-1})	18.3	11.7	12.5	17.1

Table 3. Thermodynamical variables over the Istria peninsula for four selected cases. In the table, abbreviations represent: CAPE: convective available potential energy, CIN: convective inhibition, LCL: lifting condensation level, LFC: level of free convection. Max CAPE, max CIN, LCL and LFC are calculated for the parcel in each grid point with maximum equivalent Θ below 3000 m a.g.l. Hourly maximum values of max CAPE, max CIN and hourly minimum values of LCL and LFC were averaged between 10:00 and 14:00 CET. From vertically averaged mixing ratio (q; g kg^{-1}) and air temperature (T; ° C) in the layer of 850–500 hPa, hourly maximum q and T values (over the peninsula) were averaged in time, between 10:00 and 14:00 CET.

Parameters in horizontal cross sections (10:00–14:00 CET)	Case C1 9 Jul 2006	Case C2 8 Aug 2006	Case C3 8 Jun 2003	Case C4 6 Jul 2009	Case C4 7 Jul 2009
max CAPE (J kg^{-1})	1780	1260	3332	2063	2699
max CIN (J kg^{-1})	29	66	78	63	79
LCL (m)	1060	793	746	432	277
LFC (m)	1133	820	908	477	356
Averaged max q (g kg^{-1}) between 850 and 500 hPa	6.2	4.7	4.3	6.4	6.8
Averaged max T (°C) between 850 and 500 hPa	1.7	−1.2	2.8	2.3	1.6

(LFC $\sim$ 1100 m). In the western SB, a low-level mixing ratio (q) is approximately 13 g kg^{-1} (Fig. 5b, Table 2) which corresponds to rh $\sim$ 70 % along the peninsula. The vertically averaged q in the critical layer between 850and 500 hPa (according to the e.g. Shepherd et al., 2001; Barthlott et al., 2006) is in the range of 3–7 g kg^{-1}, as shown in Table 3. These q values correspond to rh values that are in general higher than 50 % (Fig. 5c). In accordance with the described atmospheric conditions, the CAPE and low-level q values are somewhat less than reported as favourable conditions for convective activity over a low-mountain range in SW Germany (CAPE $\sim$ 2500 J kg^{-1} and low-level $q \sim 18$ g kg^{-1} in Barthlott et al., 2006). Nevertheless, Shepherd et al. (2001) argued that at least 60 % relative humidity in the Florida lower troposphere was favourable enough for thunderstorm development, which corresponds to the results shown here.

The initial Cb development occurred over the mountain ridges (Fig. 4), where the main cause of their origin was the larger air lifting along the slopes and well-disposed atmospheric humidity in the mid-troposphere. The Cb cells propagated toward the downslope side providing the rapid development of new convective cells over the peninsula. Two features were very important for the significant development of the thunderstorm: (i) cloud advection by the NE ambient wind and (ii) the existence of the low-level convergence zone. From 10:00 to 12:00 CET, the initial cells over the mountains were advected by the NE wind to the SW, positioning them to the leeward side of the mountain range relatively close to the NW part of the surface convergence zone. In this area, during their mature phase (at 11:00 CET, Fig. 4b), the downdraught outflows from the convective cells collide with an SB front along the convergence zone, elevate humid air from SB and make secondary cells along the NW part of peninsula. Cells were usually separated by distances of $\sim$ 10 km. Kingsmill (1995) noted that a certain distance between the gust fronts and SB fronts must exist for the strongest convergence and convective development. He suggested an optimal extent of approximately 7 km on either side of the initial boundary contact point for this distance.

With the cell creation above the convergence zone, the forced propagation mechanism of the storm's movement along the convergence zone toward the south is established. According to Cotton et al. (2011), forced propagation means the sustained regeneration of a convective storm by an external forcing mechanism, such as the SB fronts and convergence zone here. In the early afternoon, fed by western SB, the new cells started to bud and the explosive development over the centre of the peninsula occurred (Fig. 4c, g). During this stage close to Pazin, the cloud-top height is approximately 8 km, with updraughts that reach 11 m s^{-1} at approximately 5 km aloft. The downdraughts were asymmetric on the side opposite to the SB at first (in Fig. 5d $\sim$ 1.8 m s^{-1}). The downdraughts (up to 3.3 m s^{-1} at 850 hPa level in next hour) created two relatively large pools of cold air (of approximately 2–3 °C) beneath the cloud bases that affected the separation from their origin within the SB front (not shown). After 14:00 CET, the convective activities were in the decay stage followed by the significant changes in the near-surface wind (and therefore the SB flow), temperature and humidity over the peninsula.

3.2 Case with the NW large-scale wind (case C2)

In this case, the NE Adriatic was mostly affected by the rear side of the eastward moving cyclone, while the western Adriatic coast was under the influence of the cyclone that simultaneously developed in the Bay of Genoa (Fig. 6a). Due to the Genoa cyclone, the synoptic set-up in this case differs from the previous one, causing more pronounced pressure gradients over the area of interest. Since the NE Adriatic was at the rear side of the upper-level trough, along the eastern Adriatic (i.e. in Udine and Zadar), the pre-storm environmental wind was predominantly from the NW direction with speeds mostly below 10 m s^{-1} in the first 6 km of the troposphere (Fig. 6b). While above the Udine station at 00:00 UTC, the

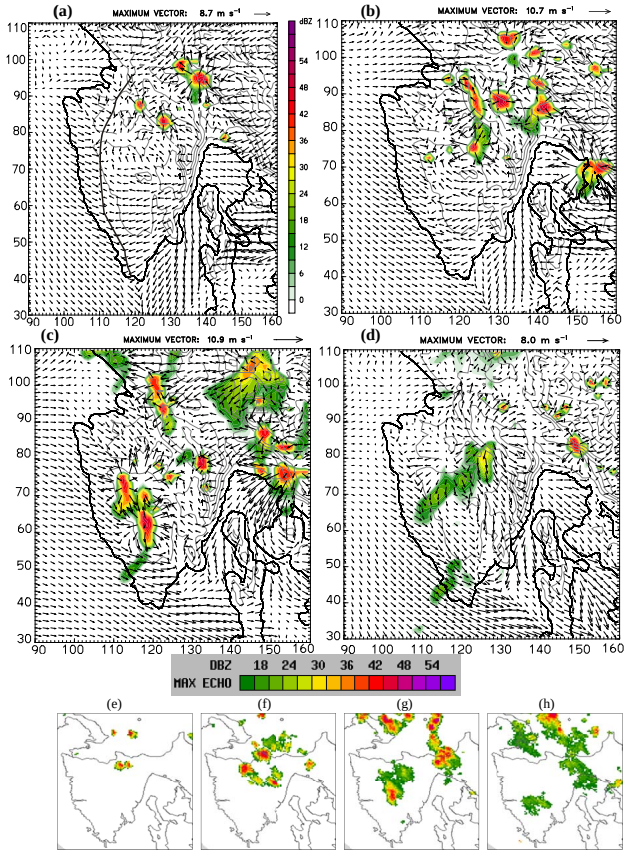

Fig. 4. (a–d) Diurnal evolution of the modelled near-surface wind (in $m\,s^{-1}$, at 10 m a.g.l.) associated with the maximum simulated equivalent radar reflectivity factor (dBZ) on 9 July 2006 at **(a)** 10:00 CET, **(b)** 11:00 CET, **(c)** 14:00 CET and **(d)** 16:00 CET. Wind vectors are depicted on every second grid point (reference length in the upper right corner-hand corner). The thick black solid line in **(a)** indicates the position of the main convergence zone. **(e–h)** Radar reflectivity factor (dBZ) in radar images (source: ARSO – www.meteo.si) on 9 July 2006 at **(e)** 11:00 CET, **(f)** 12:30 CET, **(g)** 13:30 CET and **(h)** at 14:30 CET. The radar reflectivity is given with a 3 dBZ interval.

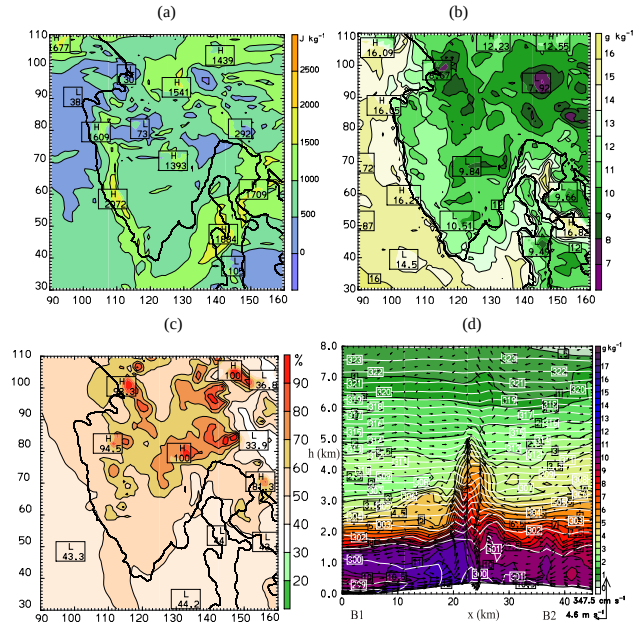

Fig. 5. Horizontal distributions on 9 July 2006 of **(a)** the CAPE ($J\,kg^{-1}$) at 10:00 CET that represents the potential for deep convection; **(b)** the low-level humidity mixing ratio ($g\,kg^{-1}$) at 13:00 CET; **(c)** the averaged relative humidity (%) in the layer between 850 hPa and 500 hPa at 12:00 CET; **(d)** vertical cross-section (B1B2) (in Fig. 1a) of the potential temperature (while lines), humidity mixing ratio (filled areas) and wind vectors at 13:00 CET.

large potential energy for the convection was present in the convective indices (CAPE $\sim 900\,J\,kg^{-1}$, CIN $\sim -87\,J\,kg^{-1}$, and BRN > 50), in Zadar and later in the day along the coast, these magnitudes were significantly decreased (with e.g. CAPE $< 200\,J\,kg^{-1}$ at both stations). Still, the convection over the NE Adriatic is confirmed by the clouds over the mountaintops in the noon satellite image revealing simultaneously the nearly straight line of midday clouds over the peninsula (not shown). This cloudy line was associated with the early afternoon lightning distribution, visible as a v-stripe shape in Fig. 6c. The v-stripe corresponds to the surface convergence of the relatively rare surface wind measurements (Fig. 6d). Despite the deep moist convection, there is no recorded precipitation in Pazin (Table 1).

At 10:00 CET, the SB developed on the shores of the peninsula according to both measurements (Fig. A1) and the model (Fig. 7a). In some areas, such as the Gulf of Trieste and along the western Istrian coast, the SB system overlapped with the ambient wind causing the advection of the sea air inland (Fig. 7a, b). The SE coast, however, was influenced by the less organised weak wind regime that was difficult to simulate precisely enough. Until 13:00 CET, the SB intrusion over land is sporadically greater than 40 km in the northern part of the peninsula and decreases to the south. The main convergence zone was strongly curved in space as a result of the western and SE onshore flow collision. Due to the overlap in directions between the large-scale wind and SB flow, the SB front strength is decreased in terms of the surface convergence (Table 2), SB front height and updraft speeds. If a deeper SB penetration and larger horizontal SB wind speeds (Fig. 7a, b) were not accompanied by greater vertical velocities at the SB front and by vertical SB dimensions (Table 2), SB systems were defined as weak(er). Therefore, this case represents thunderstorm case supported by the weak(est) SB event.

The life span of a thunderstorm event (Fig. 7) is approximately 6 h starting at approximately 11:00 CET and decaying at 16:30 CET, with a slight delay (by 1 h) in the model. Around noon (Fig. 7a, e), the daytime radar images show two

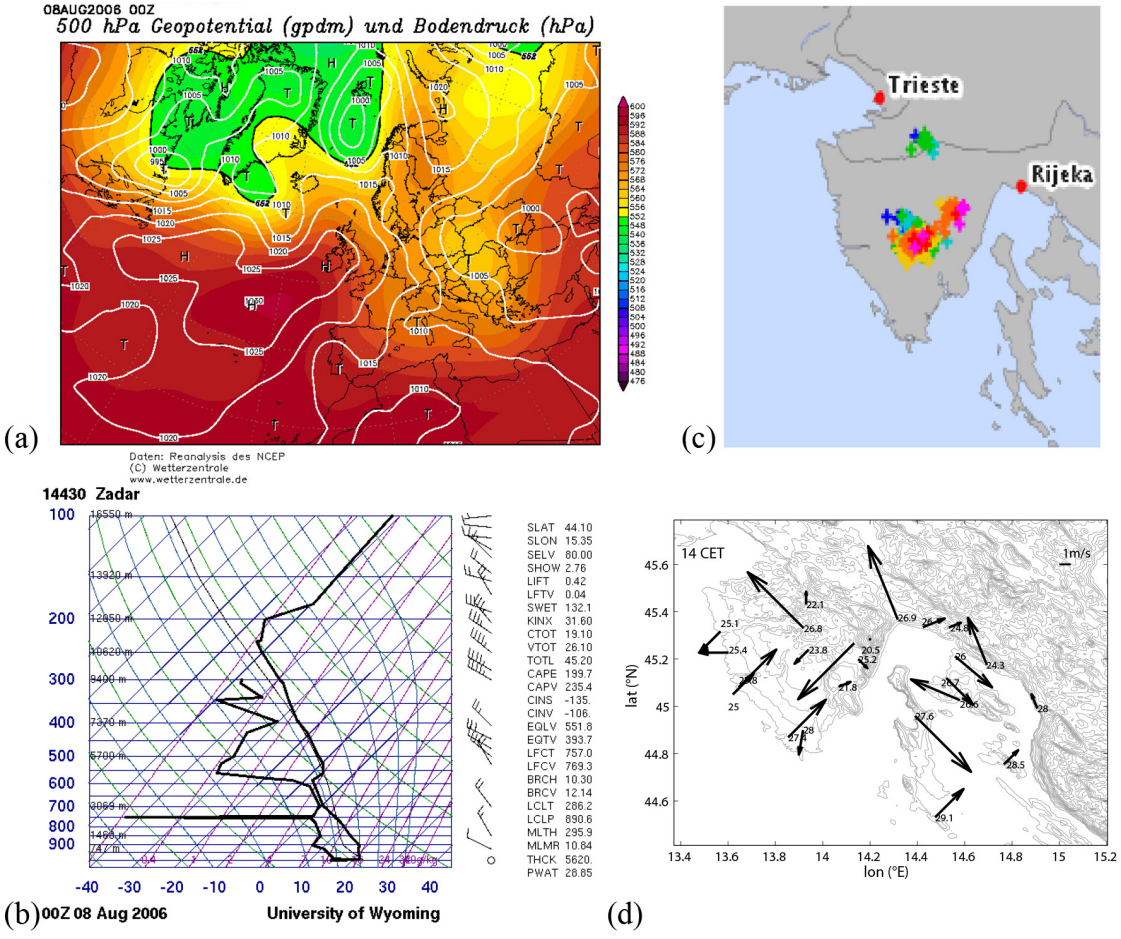

Fig. 6. Case C2, 8 August 2006: **(a)** surface and 500 hPa pressure distribution at 00:00 UTC (= 01:00 CET); **(b)** radio sounding profiles plotted on a skew T-log p diagram in combination with convective indices in Zadar (44.10° N/15.35° E) station at 00:00 UTC (= 01:00 CET); **(c)** lightning distribution from 13:00 to 14:00 CET from LINET network (Betz et al., 2009). The coloured crosses indicate the detection of lightning, same as in Fig. 2c; **(d)** the measured 10 m wind vectors ($m\,s^{-1}$) and 2 m air temperatures (°C) at 14:00 CET (measuring sites in Fig. 1a).

independent regions of significant convective activity (that are partially reproduced by the model): a mountainous area to the north and a prominent convex part of the SE Istrian coast. A blocking effect of the northern mountains resulted in a significant uplift of the NW flow that triggered the thermal convection over the elevated (Učka) area. Although the model limitations unfortunately did not allow a perfect reproduction of all Cb cells, it seems that the surface convergence, augmented by the curved part of the coastline, initiated the SE storm cell.

Case C2 is characterised by the lowest CAPE and the lowest near-surface humidity compared to the other cases (Tables 2 and 3). Nevertheless, the mid-tropospheric humidity over the peninsula was consistently high (Fig. 8b), satisfying the favourable conditions for thunderstorm development (Shepherd et al., 2001). The horizontally tilted zone of maximum CAPE in Fig. 8a was determined by the horizontally tilted zone of narrow low-level convergence (Fig. 7a) and corresponds to the cloud line in the satellite image (not shown). At 13:00 CET, both the model and the observations showed several storm cells developing (Fig. 7b and f). Apart from the storm cell intensification over the mountain of Učka, in the middle of the peninsula, convective cells occurred above a convergence zone. The thunderstorm outflow collision of sporadic cells with the SB fronts along the convergence zone produced new, stronger convection over the larger part of peninsula; the convection is visible as a v-stripe (Fig. 7c and g) where the high reflectivity areas correspond to the highest density lightning areas (Fig. 6c). The downdraughts spread out downwind rapidly creating a cold pool of drier and colder air (up to 4 °C colder) from the high levels that destroyed the suitable conditions for the SB maintenance. The interaction between the gust front and SB front was also the main mechanism responsible for the afternoon occurrence of new storm cells in the NW of the peninsula (Fig. 7d and h). According to the path of convective cells

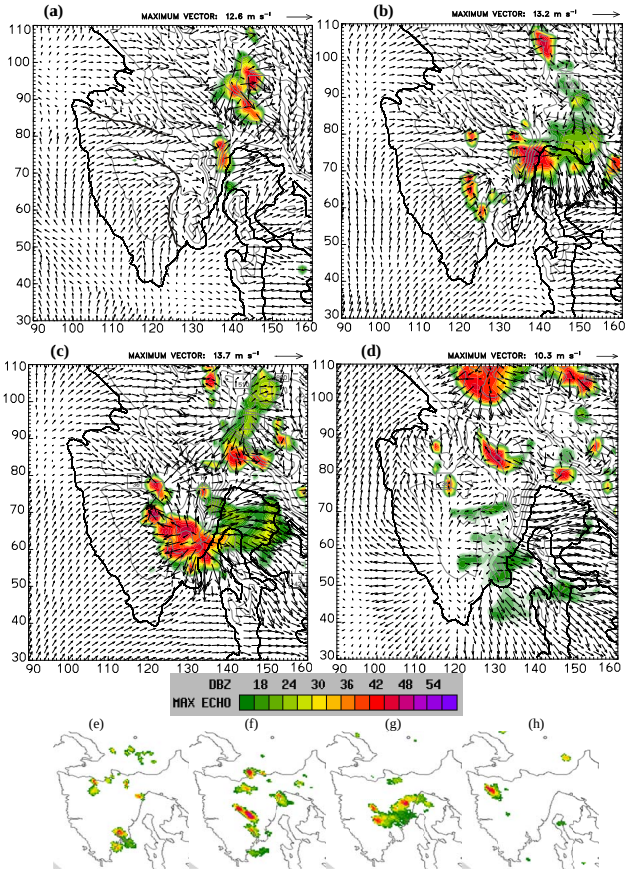

Fig. 7. (a–d) Diurnal evolution of the modelled near-surface wind (in $\mathrm{m\,s^{-1}}$, at 10 m a.g.l.) associated with the maximum simulated equivalent radar reflectivity factor (dBZ) on 8 August 2006 at **(a)** 12:00 CET, **(b)** 13:00 CET, **(c)** 14:00 CET and **(d)** 16:00 CET. Wind vectors are depicted in every second grid point (reference length in the upper right corner-hand corner). The thick black solid line in (a) indicates the position of the main convergence zone. **(e–h)** Radar reflectivity factor (dBZ) in radar images (source: ARSO – www.meteo.si) on 8 August 2006 at **(e)** 11:10 CET, **(f)** 13:00 CET, **(g)** 13:50 CET and **(h)** at 15:30 CET. The radar reflectivity is given with a 3 dBZ interval.

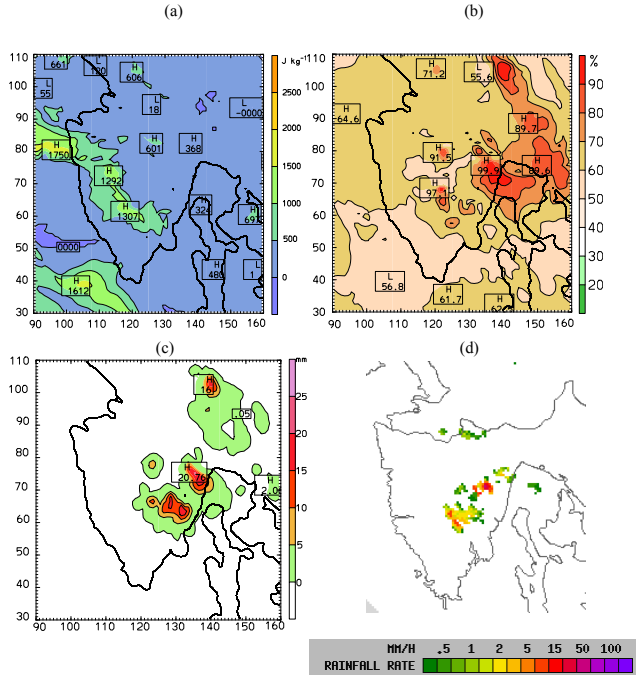

Fig. 8. Horizontal distributions on 8 August 2006 of **(a)** the CAPE ($\mathrm{J\,kg^{-1}}$) at 12:00 CET that represents the potential for deep convection; **(b)** the averaged relative humidity (%) in the layer between 850 hPa and 500 hPa at 13:00 CET; **(c)** total precipitation (mm) from 13:00 to 14:00 CET total precipitation in past 1 h; **(d)** rainfall rate at 13:40 CET (source: ARSO – www.meteo.si).

spreading, this is a case where the gust front-SB front interactions overcome the effect of large-scale NW wind advection on convective clouds. Over the Bay of Rijeka, storms dissipated quickly when they moved over the sea due to the increased stability. The total rainfall was slightly higher than the estimated radar value; however, the location and distribution of rainfall was generally tied to the convergence zone in both the model (Fig. 8c) and measurements (Fig. 8d). The lower mixing ratio that existed in the colder air (compared to the case C1) still produced unstable convergent SB updraughts. Consequently, the three-dimensional overshooting uplifts sporadically exceed $11\,\mathrm{m\,s^{-1}}$ (at 4 km aloft) with the cloud-top at 9.5 km that made case C2 the most intense thunderstorm case.

3.3 Cases with onshore large-scale wind (cases C3 and C4)

On 8 June 2003 (C3 case), a high-pressure field with weak surface pressure gradients was situated over the NE Adriatic (Fig. 9a), being a part of a large anticyclone with centre over the central Europe. In the vertical, high-pressure field was stretching all the way up to 200 hPa, making the flow at the NE Adriatic region generally SE to southern throughout the troposphere (Fig. 9b). Speeds were less than $7\,\mathrm{m\,s^{-1}}$ below 10 km, and above 600 hPa level to the tropopause the winds were very persistent with small directional changes, less than 50°. A shallow elevated cyclone over Sardinia also supported these flow directions over the Adriatic. Similar to the case C1, diffluent flow in Fig. 9a, with very weak pressure gradients also in the upper levels, can be observed over the central Europe region. At 00:00 UTC, the sounding in Zadar shows a prominent maximum in temperature at about 900 hPa (Fig. 9b). As a consequence of the warming in the daytime, soundings at noon at both locations show a conditionally very unstable atmosphere with large CAPE values $\sim$(900–1300 $\mathrm{J\,kg^{-1}}$), with CIN $\sim$((−50)–(−80) $\mathrm{J\,kg^{-1}}$) and BRN in the range of 103 (Zadar) and 858 (in Udine). Thunderstorm characteristics (e.g. lightning flashes) for this particular case are displayed in Fig. 9c, with Cb formation and

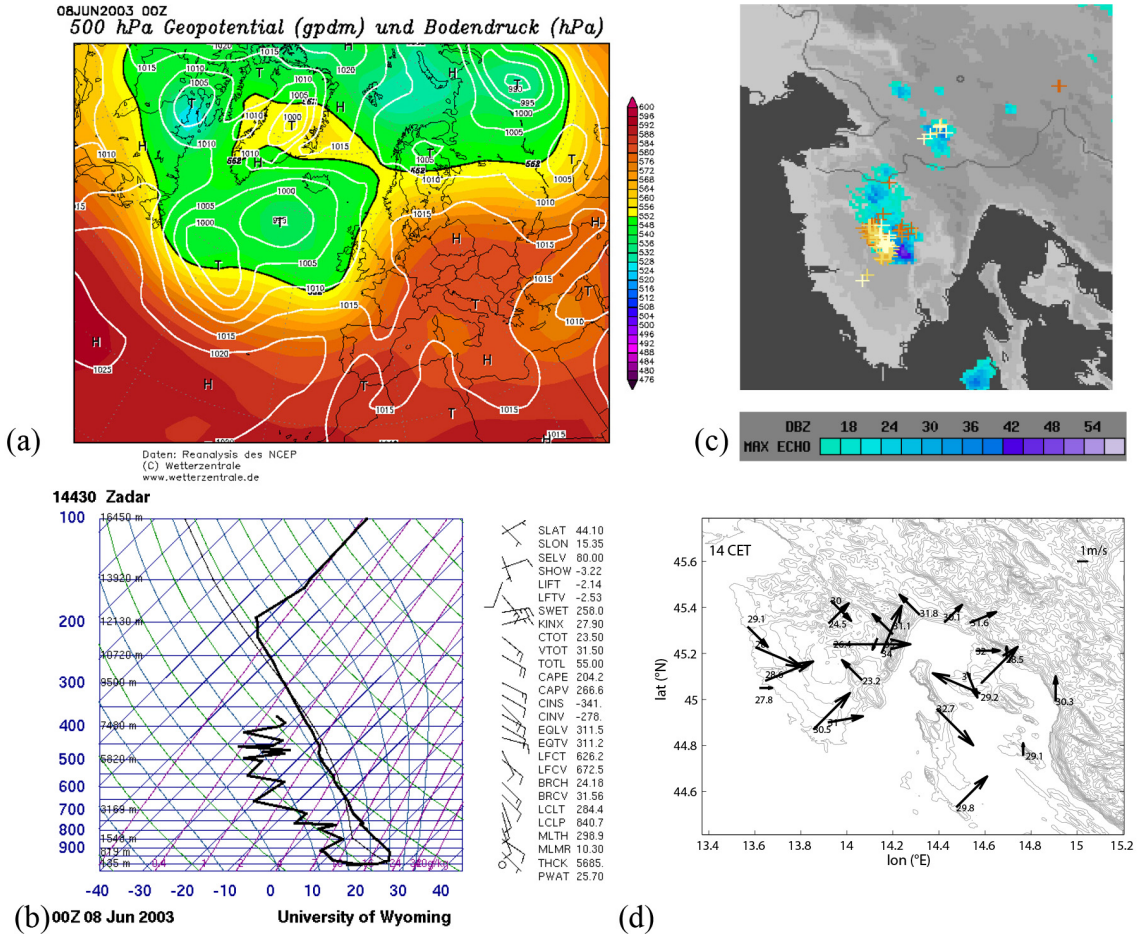

Fig. 9. Case C3, 8 June 2003: **(a)** surface and 500 hPa pressure distribution at 00:00 UTC (i.e. 01:00 CET); **(b)** radio sounding profiles plotted on a skew T-log p diagram in combination with convective indices in Zadar (44.10° N, 15.35° E) station at 00:00 UTC (i.e. 01:00 CET); **(c)** cloud-to-ground lightning distribution (crosses), from 13:00 to 14:00 CET and radar echo (blue areas); source: ARSO – www.meteo.si (Slovenian Environment Agency). The coloured crosses indicate the detection of lightning: yellow (< 10 min) – orange (> 50 min); **(d)** measured 10 m wind vectors ($m\,s^{-1}$) and 2 m air temperatures (°C) at 14:00 CET (measuring sites in Fig. 1a).

precipitation occurring in the middle of the peninsula (Table 1). The NE Adriatic coast was influenced by the undisturbed SB flow with speeds up to 4.5 $m\,s^{-1}$ that are observed in the measurements (Fig. 9d) and confirmed by the model (Appendix A).

The last chosen case (C4 case) belongs to the most frequent convective weather type, in nearly 50 % of all observed cases associated with deep moist convection in the NE Adriatic (Mikuš et al., 2012). It is characterised by the approaching of a large deep cyclone from the NW over western Europe with formed low in the Bay of Genoa (Fig. 10a). These low pressure formations were destroying the existed NG weather type over the NE Adriatic on 6 July 2006. They caused a rotation of large-scale wind direction from NE to SW that contributed to the significant moisture intrusion over the land. According to the soundings in Zadar, Fig. 10b, the SW to WSW wind dominated in the whole troposphere and gradually strengthened from midday 6 July (to $\sim 8\,m\,s^{-1}$) to midday 7 July (to $\sim 18\,m\,s^{-1}$) below 400 hPa. The front (connected with this low) has become quite intense producing strong and relatively long-lasting convection (Table 1) and severe weather over much of the NE Adriatic. In the morning hours on 7 July hail was reported over the Pula airport. While convective indices (Fig. 10b) confirmed convection over the area of interest, SB and its characteristics were less obvious over the peninsula (Fig. A1). According to the surface measurements, while the SB was blowing inland over Istria during 6 July (similarly to case C3; not shown), the relatively uniform landward flow in Fig. 10c does not present a developed SB (if at all) over the peninsula on 7 July, which will be discussed in the following sections. This synoptic set-up, associated with the SB–Cb phenomena that occurred upstream of the approaching trough under the influence of moderate SW flow, is quite typical in the western Mediterranean as well (Barthlott and Kirshbaum, 2013).

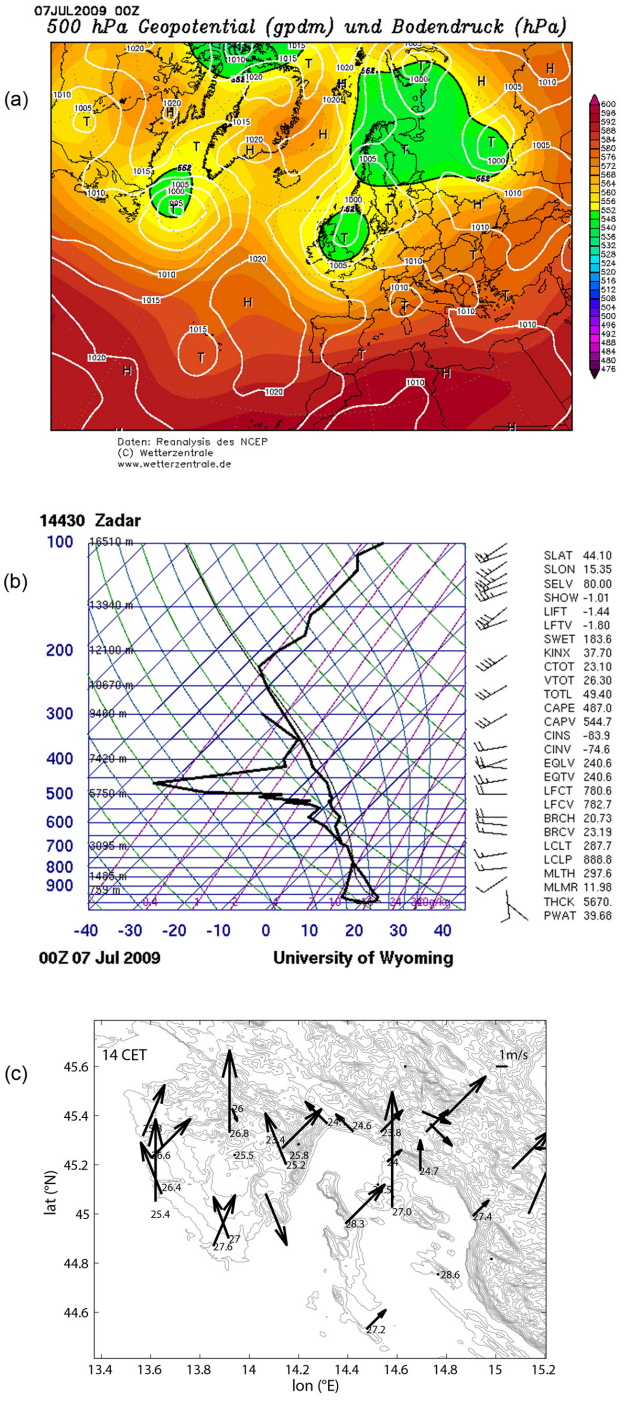

Fig. 10. Case C4, 7 July 2009: **(a)** surface and 500 hPa pressure distribution at 00:00 UTC (i.e. 01:00 CET); **(b)** radio sounding profiles plotted on a skew T-log p diagram in combination with convective indices in Zadar (44.10° N, 15.35° E) station at 00:00 UTC (i.e. 01:00 CET); **(c)** measured 10 m wind vectors ($m\,s^{-1}$) and 2 m air temperatures (°C) at 14:00 CET (measuring sites in Fig. 1a).

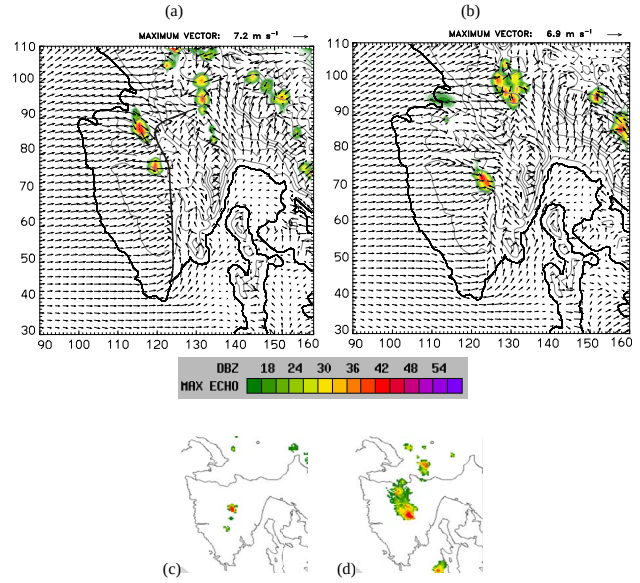

Fig. 11. (a, b) Diurnal evolution of the modelled near-surface wind (in $m\,s^{-1}$, at 10 m a.g.l.) associated with the maximum simulated equivalent radar reflectivity factor (dBZ) on 8 June 2003 at **(a)** 13:00 CET and **(b)** 14:00 CET. The every second wind vector is depicted with reference vectors near the upper right-hand corner and the thick black solid line in **(a)** indicates the position of the main convergence zone. **(c, d)** Radar reflectivity factor (dBZ) in radar images (source: ARSO – www.meteo.si) on 8 June 2003 at **(c)** 12:50 CET and **(d)** 14:00 CET. The radar reflectivity is given with a 3 dBZ interval.

In cases C3 (Fig. 11) and C4 (Fig. 12), the southerly ambient winds are mostly onshore, which could produce a much deeper inland SB intrusion (Miller et al., 2003). In the model, the western SB is very well developed, with penetrations of 35 km inland in the early afternoon that occur almost uniformly along the peninsula (see Figs. 11b, 12b). The SE part of Istria is marked by the weak SB in C3 and almost ill-defined in C4 (with many local convergence zones), still forming the interior convergence zone along the peninsula. In addition to the afternoon deepest intrusion of the western SB over land (Table 2), the onshore ambient wind determined the width of the SB front and (lower) vertical updraft along it.

The lifetime of C3 stormy event along the peninsula is relatively short according to both the model and the radar data (Fig. 11); from 12:40 CET to 15:00 CET with its culmination at approximately 13:30 CET. The comparison between the modelled and measured radar reflectivity revealed a relatively correct daytime evolution and duration of the modelled event; however, the spatial coverage is underestimated by the model during the maximum phase of thunderstorm event.

Among the cases (Table 3), the CAPE in C3 along the convergence zone had the largest values ($\sim 3000\,J\,kg^{-1}$) and, consequently, the lower LFC and LCL which means in order

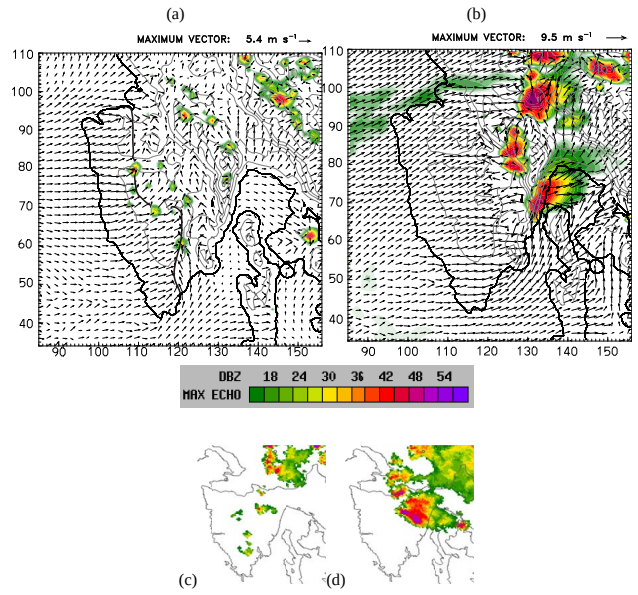

Fig. 12. (a, b) Diurnal evolution of the modelled near-surface wind (in $m\,s^{-1}$, at 10 m a.g.l.) associated with the maximum simulated equivalent radar reflectivity factor (dBZ) on 6 July 2009 at **(a)** 11:00 CET and **(b)** 14:00 CET. The every second wind vector is depicted with reference vectors near the upper right-hand corner and the thick black solid line in **(a)** indicates the position of the main convergence zone. **(c, d)** Radar reflectivity factor (dBZ) in radar images (source: ARSO – www.meteo.si) on 6 July 2009 at **(c)** 10:50 CET and **(d)** 14:00 CET. The radar reflectivity is given with a 3 dBZ interval.

to trigger convection a faster uplift is required. The largest modelled CAPE is consistent with the potential for the convection observed for the radio sounding data in this case as well. The spatial distribution of CAPE along the peninsula (not shown) is similar to that in case C1 (Fig. 5a), still with smaller differences. In case C1, the convergence in the wind field and larger CAPE are in the southern part of the peninsula. In contrast, in C3, a stronger merging of the near-surface wind is in the NW part of the peninsula (Fig. 11a) producing higher CAPE (and consequently the Cb cell). The main reason is the divergence of the onshore flow due to the concave coastline in the Gulf of Trieste and increased surface roughness over the land.

While the model reproduced the observed highest low-level humidity in case C3 (Tables 2 and A1), it simultaneously revealed a significant decrease in the moisture above the boundary layer (PBL) height (Figs. 13a, b). The vertically averaged (850–500 hPa) rh values mostly in the range of 20–40 % indicated a relatively dry atmosphere aloft. In such an atmospheric environment, the SW to westerly surface flow favours only the development of sporadic convection above the convergence zone, as shown in Fig. 11. In this case, the enhanced low-level humidity ($q \sim 15$–$16\,g\,kg^{-1}$) close to the SB front position and associated overshooting updraft (with speeds greater than $11\,m\,s^{-1}$) over the convergence zone resulted in several short-lived single Cb cells in the model. However, despite the existence of downdraughts and cold pools of air (at approximately 1–2 °C) beneath the cloud base, the influence of cells on the thermodynamic fields was only minor. The intensity of the precipitation was rather rare and sporadic over the peninsula (not shown).

According to the model, the main driving mechanism for deep convection initiation and maintenance in case C3 was (i) the lower-tropospheric shear along the convergence zone and (ii) the humidity advection by the SB front. The latter elevates both the amount and the depth of humidity in the mid-troposphere very locally in the presence of mid-level subsidence (due to high pressure environment). The dry air entrainment could reduce cloud buoyancy by evaporating water (Sherwood et al., 2010). Although the model underestimated the thunderstorm intensity, compared with the other cases, case C3 also had the shortest duration and the smallest spatial dimensions according to the radar images. Bearing in mind that convective development needs three main ingredients: moisture, instability and lift (Doswell III, 1987), in this case, one of the ingredients, namely mid-tropospheric moisture, seems to be below average amount for strong stormy events (Table 3). Since instability was present (according to the instability indices derived from the radio soundings and confirmed by the model) and lift is provided primary by the low-level wind convergence and by the orography of Istria, it can be presumed that under-average mid-tropospheric moisture is compensated by the SB mechanism advecting humid air from the sea in the lowest layers.

Weak storm intensity in C3 provokes the question: how much is C3 really a typical thunderstorm case for the NE Adriatic? Mikuš et al. (2012) stressed that the SW wind regime on the front side of low pressure systems dominated in lightning climatology as atmospheric background for thunderstorms. They defined a thunderstorm day as a day with at least 10 lightning strokes per hour (regardless of time of day) across the NE Adriatic. As daytime Cb development is the focus here, we performed the additional (re)analysis of weather types and wind regimes based on the same methodology as in Mikuš et al. (2012). Accordingly, we have selected 100 days with daytime Cb and/or only daytime lightning (see Sect. 2.2) in the warm period from 2000 to 2009. The reanalysis of thunderstorm database showed that when the potential SB–Cb interaction occurred, NW and NE wind regimes were almost always products of remote low pressure systems and were much more frequent as atmospheric conditions (than in Mikuš et al., 2012). This means in ∼ 60 % of SB–Cb days (Fig. 14). In addition, the NE wind usually advects less cold air from the Black Sea area, and the NW wind brings much colder air from the Atlantic/north that agrees to the mid-tropospheric temperatures in Table 3. The situation is also different regarding the landward wind directions, where in almost ∼ 40 % of all onshore synoptic wind cases, the formation of high pressure pattern exists above NE

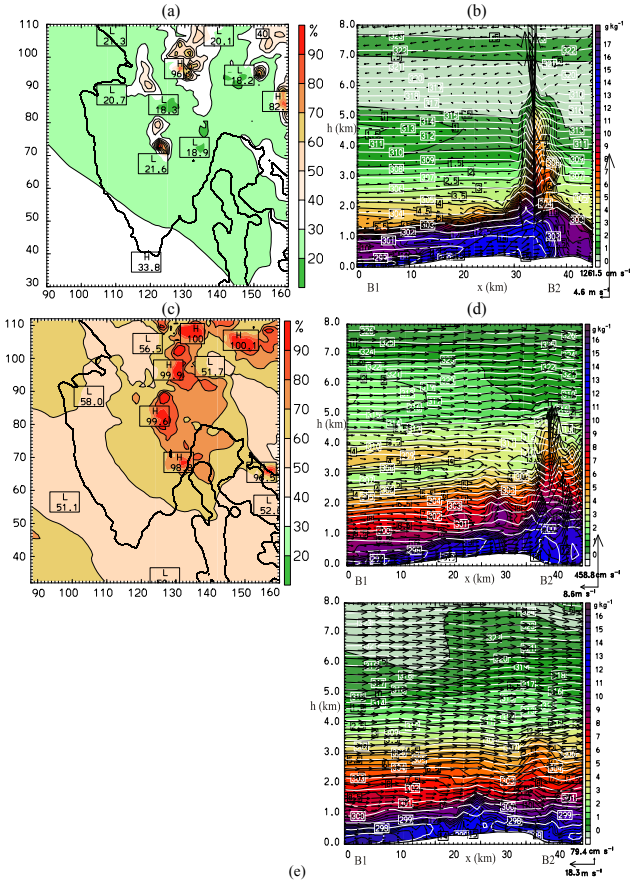

Fig. 13. (a, c) Horizontal distributions of the averaged relative humidity (%) in the layer between 850 hPa and 500 hPa at 14:00 CET on **(a)** 8 June 2003 and **(c)** 6 July 2009; **(b, d, e)** vertical cross-section (B1B2) (see in Fig. 1) of the potential temperature (white lines), humidity mixing ratio (filled areas) and wind vectors at 13:00 CET on **(b)** 8 June 2003, **(d)** 6 July 2009 and **(e)** 7 July 2009.

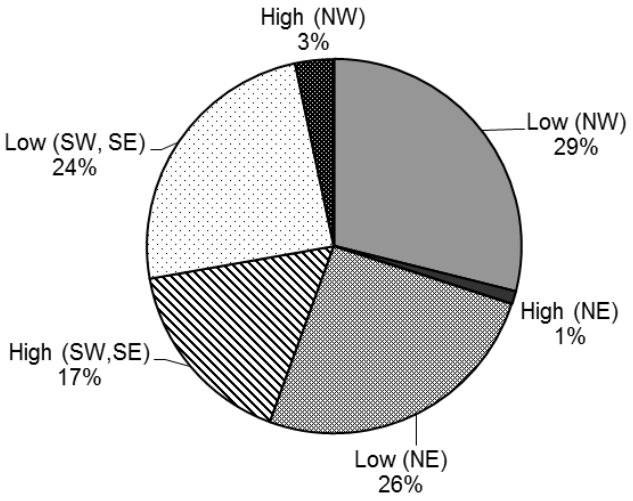

Fig. 14. A relative proportion of days with particular atmospheric conditions with daytime thunderstorm occurrence during 2000–2009 warm seasons over the NE Adriatic for four large-scale flows: NE, NW, SE, SW generated by the low- and high-pressure systems.

Adriatic. There are several reasons for the reduced number of the most common SW warm-wet flow in cases with SB–Cb interaction. First, the Mediterranean cyclones are more frequent during spring and autumn when SBs are less frequent (Prtenjak and Grisogono, 2007), with significantly lower incidence in summer. Second, the eastward tracks of Mediterranean cyclones (e.g. Horvath et al., 2008) actually mean further strengthening of the large-scale flow over the target area that consequently prevents the SB development over Istria. This can be seen in the SB evolution in case C4 which despite the warm temperature advection and very favourable moisture distribution in the unstable flow (the largest mid-tropospheric humidity and large CAPE; the lowest LCL and LFC; Table 3 and Fig. 13c–e), the initially formed convergence zone in the late morning (Fig. 12a) rapidly lost its basic features (shown in cases C1–C3). Due to the overlapping between the western SB and SW large-scale wind, the convergence zone moved very fast toward the NE of the peninsula in the base of the mountains (Fig. 12b). The convective activity existed further due to gust front interactions, and new convective cells (followed by the rainfall pattern) were quasi-stationary over the upwind slopes and over the highland area with cold pool beneath (up to 5 °C colder). Additional increase in synoptic wind speeds disrupted further development of local circulations during the afternoon and particularly on the following day (Fig. 13e).

3.4 Some parameters relationships

In order to analyse the effect of the different synoptic flows on the SB flow and convective potential over peninsula Fig. 15 showed the relationship between kinetic energy (KE) of the large-scale wind and CAPE (Fig. 15a) as well as KE of the large-scale wind and low-level convergence across convergence zone (Fig. 15b). Recently Miglietta and Rotunno (2009) have shown, that a non-dimensional number CAPE/speed^2 represents the ratio of the control parameters (still considering idealised conditions) that can display the effect of the orography on a conditionally unstable flow. Here four points in the smallest domain (Pazin, S1, S3 and S4 in Fig. 1a) were chosen since they were almost equally distant from the nearest mountain ridge and for each large-scale direction presented upstream and downstream atmospheric conditions. In all simulated days, in every hour between 09:00 and 19:00 CET, 1-D profiles of real cases were used to estimate maximum wind speed (Vm) (i.e. KE max (= Vm^2/2)) in the layer of 850–500 hPa and maximum CAPE. Their quite regular relationship, shown in Fig. 15a, reveals that in general, larger KE max decreases with CAPE and vice versa that could be defined by power law. However, while this relationship is valid only for the days with SB–Cb interaction, during the day without SB and

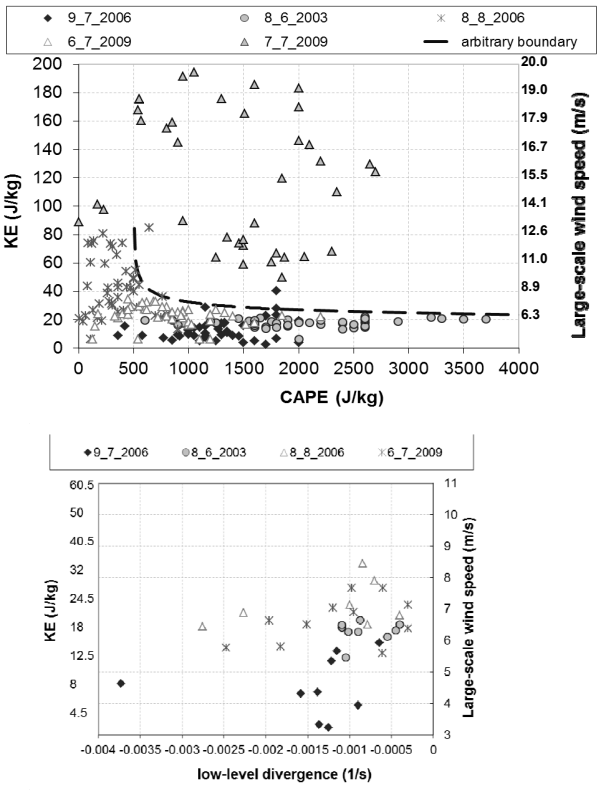

Fig. 15. (a) Relationship between maxima kinetic energy (KE) of the large-scale flow and the maxima CAPE, calculated for 1-D profiles in four points (Pazin, S1, S3 and S4 in Fig. 1) in the finest model domain. Each symbol represents relationship for every hour between 09:00 and 19:00 CET for each day of all four cases (C1–C4). The KE maxima are calculated (i.e. $Vm^2/2$) according to the maxima horizontal wind speed (Vm) in the layer between 850 and 500 hPa. A bold dashed line displays arbitrary boundary between SB and Cb occurrence and only Cb occurrence. **(b)** Relationship between Vm above Pazin and low-level divergence calculated along B1B2 vertical cross section. As seen in **(a)** each symbol represents relationship for every hour between 09:00 and 19:00 CET for each day of all four cases (C1–C4) in the smallest domain.

only Cb occurrence (7 July 2009) the scattering of this relationship is considerably larger. In fact, dissipation is such that any significant matching cannot be found. The modelled data (based on four cases) suggest an arbitrary boundary (black dashed line) between these two regimes for the NE Adriatic; for example, for CAPE larger than $500\,\mathrm{J\,kg^{-1}}$ (as lower boundary), the maximum large-scale wind speed smaller than $9\,\mathrm{m\,s^{-1}}$ below 500 hPa would allow SB occurrence and SB–Cb interaction.

Since large-scale wind highly influences the position and duration of the convergence zone, in Fig. 15b the relationship between KE max for Pazin (for winds in the range of 850 and 500 hPa level) and the low-level divergence over convergence zone along cross-section B1B2 is displayed. The horizontal divergence values are of the order of magnitude about $-1\times10^{-3}\,\mathrm{s^{-1}}$ which is in agreement with values obtained from radar data for initiating surface-based thunderstorms (Banacos and Schultz, 2005). The relationship presents simultaneously the influence of both the synoptic and mesoscale scales. Although, it is based on a small sample since lifetime of the convergence zone in the afternoon hours is mostly over, the existence of the convergence zone in days with SB–Cb interplay revealed several things. They are (i) the convergence zone intensity partially depends on the large-scale wind direction (compare e.g. C1 and C3), (ii) larger synoptic wind speeds in general indicates smaller intensity of convergence zone, and (iii) the upper boundary for the large-scale wind speed (above PBL) for the occurrence of the convergence zone in PBL is less than $9\,\mathrm{m\,s^{-1}}$.

To investigate influence of the convergence zone further, one measure called the low-level moisture flux convergence (MFC; Eq. 5 in Banacos and Schultz, 2005) is used since it can serve for the short-range forecast of convection along well-defined surface boundary. It consists of two contributions showing "moisture pooling" and forced lifting: the horizontal advection of humidity and horizontal divergence term (multiply by humidity). In Table 2, MFC is calculated along B1B2 vertical cross section in accordance with its definition. MFC values associated with the SB front are in the range of 11 to $19\times10^{-3}\,\mathrm{g\,kg^{-1}\,s^{-1}}$ and they correspond to those values estimated in the vicinity of convective initiation in severe-storm observational studies (Banacos and Schultz, 2005). It was observed that the MFC magnitudes were greatly affected by the effect of the divergence term and, accordingly, the highest values are in case C1. Still, comparing equal values for divergence in cases C2 and C3, the MFC parameter in C3 confirm potential for the thunderstorm development due to the largest contribution of low-level humidity and its advection.

4 Summary and conclusions

The diurnal evolution of four individual summer cases over the NE Adriatic area was investigated by available measurements and simulated by the WRF model with a focus on (i) the Cb and SB interplay and (ii) variations in the amount of convective activity. The selected cases were characterised by a synoptic-gradient wind from the NE (case C1, 9 July 2006), NW (case C2, 8 August 2006), SE (case C3, 8 June 2003) and SW (case C4, 6–7 July 2009). The mesoscale model reproduced very satisfactory thermodynamical atmospheric fields (e.g. Appendix A). Because simulations of the deep convective events still represent a significant challenge for numerical forecasting (e.g. Weisman et al., 2008; Sherwood et al., 2010), certain discrepancies found between the model and observations in the lifetime, intensity and location of the deep convection characteristics still did not impede deeper analysis.

In the majority of simulated days (except 7 July 2009), typical near-surface wind patterns for the Istria region (e.g. Prtenjak et al., 2006) were reproduced, that is, SBs along the coastline and eastward-moving convergence zone. During the daytime, the narrow convergence zone formed mostly as the result of western and southeastern SBs merging along the peninsula. Each day, storms gained maximum intensity in the afternoon, thus indicating the importance of diurnal heating over the peninsula. If deep moist convection was permitted, the western SB was dominant feature in the afternoon.

Among all the cases, case C3 represented the shortest and weakest thunderstorm event, with the highest low-level moisture, relatively unfavourable mid-tropospheric humidity associated with the presence of mid-level subsidence (due to high pressure synoptic background). The origin and the Cb cell locations were completely controlled by the main elongated convergence zone and by both horizontal low-level moisture convergence and upward moisture advection by the SB front. This case, in which middle tropospheric dry layers inhibit significant deep convection, represents atmospheric conditions that are still burdened by high uncertainty in the short-term convective forecast (Banacos and Schultz, 2005). On the other hand, in the most typical case for the deep convection in the NE Adriatic that is characterised by abundant moisture in the lower and middle troposphere (case C4), SW warm-wet wind only partially support SB–Cb interaction. The reasons are the (i) deepest western SB penetration over land and/or (ii) further strengthening of the large-scale wind in time (due to the eastward tracks of the Mediterranean cyclones) that lead rapidly to the vanishing of convergence zone and locking of the moist convection over the highland area for several hours. This result indicated (and climatological reanalysis confirmed) that these atmospheric conditions are present but they are less suitable for the prolonged SB–Cb interaction.

In the examined cases (C1 and C2) that were characterised by the offshore large-scale wind, the NE mountain range accelerated the beginning of convection and influenced its intensity. A large-scale wind advection in the upper troposphere and a convergence zone in the lower troposphere had a decisive impact on the lifetimes and movements of the initial convective cells that formed over the mountain range. Along the convergence zone, the merging of SB front and thunderstorm outflow initiated new Cb cells. In case C1, the superposition of the SB front-gust front collision with the NE wind advection caused the thunderstorm to propagate southward. Despite the offshore moderate NW ambient wind in case C2 and the downwind advection of clouds until noon, the lower tropospheric interaction of the fronts determined the afternoon northwestward (opposite) movement of the storm along the peninsula. From a synoptic perspective, both landward wind types appears (as a rule) on the back/upper part of the low pressure systems that are still far enough from the NE Adriatic allowing the formation of almost NG surface pressure conditions over Istria.

Although presented cases certainly do not permit ful generalisation, they provide the possibility to form a specific background picture of the SB–Cb interplay. Favourable cases were characterised by several characteristics related to a thermodynamic environment: (i) areas with favourable mid-tropospheric moisture conditions (averaged $q > 4\,\mathrm{g\,kg^{-1}}$ and rh no less than 60 %) and/or high levels of low-level moisture in the PBL ($q > 12\,\mathrm{g\,kg^{-1}}$), (iii) large-scale wind speeds less that $9\,\mathrm{m\,s^{-1}}$ in the lowermost 6 km, (iv) instability in the atmosphere described by the CAPE $> 500\,\mathrm{J\,kg^{-1}}$, (v) positive low-level temperature difference between land and sea higher than 1.5 °C and (vi) existence of the low-level convergence (order of magnitude of $0.0003\,\mathrm{s^{-1}}$ or more). However, a further investigation of additional cases and the effects of other control parameters (e.g. terrain, SST) on the daytime thunderstorm events associated with SBs would be desirable. Moreover, to obtain the relationship of main easy-prognostic meteorological variables with other parameters of instability would be also useful. Bearing in mind that the position of the airport station is on the tip of the peninsula, the improved understanding of this type of weather event would certainly give a better real-time prediction and justify further work.

Acknowledgements. This work has been supported by the Ministry of Science, Education and Sports (grants "BORA" no. 119-1193086-1311; "AQCT" no. 119-1193086-1323; "Storms and Natural Disasters in Croatia" no. 004-1193086-3036) contributing also to the HyMeX programme. We are very grateful to the Slovenian Environment Agency for providing radar data. The second author would also like to thank Igor Tomažić for satellite images. Useful comments and suggestions from two anonymous reviewers are greatly appreciated.

Topical Editor V. Kotroni thanks two anonymous referees for their help in evaluating this paper.

References

Azorin-Molina, C., Connell, B. H., and Baena-Calatrava, R.: Sea-breeze convergence zones from AVHRR over the Iberian Mediterranean area and the Isle of Mallorca, Spain, J. Appl. Meteorol. Clim., 48, 2069–2085, 2009.

Babić, K., Mikuš, P., and Prtenjak, M. T.: The relationship between shallow thermal circulation regimes and cumulonimbus clouds along northeastern Adriatic coast, Geofizika, 29, 103–120, 2012.

Banacos, P. C. and Schultz, D. M.: The use of moisture flux convergence in forecasting convective initiation: Historical and operational perspectives, Weather Forecast., 20, 351–366, 2005.

Barthlott, C. and Kirshbaum, D. J.: Sensitivity of deep convection to terrain forcing over Medditerranean islands, Q. J. Roy. Meteorol. Soc., 139, 1762–1779, 2013.

Barthlott, C., Corsmeier, U., Meißner, C., Braun, F., and Kottmeier, C.: The influence of mesoscale circulation systems on triggering convective cells over complex terrain, Atmos. Res., 81, 150–175, 2006.

Belušić, D. and Strelec Mahović, N.: Detecting and following atmospheric disturbances with a potential to generate meteotsunamis in the Adriatic, Phys. Chem. Earth, 34, 918–927, 2009.

Belušić, D., Grisogono, B., and Klaić, Z.B.: Atmospheric origin of the devastating coupled air–sea event in the east Adriatic, J. Geophys. Res., 112, 17111–17124, 2007.

Betz, H.-D., Schmidt, K., Laroche, P., Blanchet, P., Oettinger, W. P., Defer, E., Dziewit, Z., and Konarski, J.: LINET — an international lightning detection network in Europe, Atmos. Res., 91, 564–573, 2009.

Borge, R., Alexandrov, V., del Vas, J. J., Lumbreras, J., and Rodriguez, E.: A comprehensive sensitivity analysis of the WRF model for air quality applications over the Iberian Peninsula, Atmos. Environ., 42, 8560–8574, 2008.

Carbone, R. E., Wilson, J. W., Keenan, T. D., and Hacker, J. M.: Tropical island convection in the absence of significant topography. Part I: Life cycle of diurnally forced convection, Mon. Weather Rev., 128, 3459–3480, 2000.

Challa, V. S., Indracanti, J., Rabarison, M. K., Patrick, C., Baham, J. M., Young, J., Hughes, R., Hardy, M. G., Swanier, S. J., and Yerramilli, A.: A simulation study of mesoscale coastal circulations in Mississippi Gulf coast, Atmos. Res., 91, 9–25, 2009.

Christian, H. J., Blakeslee, R. J., Boccippio, D. J., Boeck, W. L., Buechler, D. E., Driscoll, K. T., Goodman, S. J., Hall, J. M., Koshak, W. J., Mach, D. M., and Stewart, M. F.: Global frequency and distribution of lightning as observed from space by the Optical Transient Detector, J. Geophys. Res., 108, 4005, doi:10.1029/2002JD002347, 2003.

Cotton, W. R., Bryan, G., and Van den Heever, S.C.: Storm and Cloud Dynamics, 2nd Edn., Elsevier Academic Press, Oxford, 2011.

Crook, N. A.: Understanding Hector: Dynamics of islands thunderstorms, Mon. Weather Rev., 129, 1550–1563, 2001.

Crosman, E. T. and Horel, J. D.: Sea and Lake Breezes: A Review of Numerical Studies, Bound.-Lay.Meteorol., 137, 1–29, 2010.

Doswell III, C. A.: The distinction between large-scale and mesoscale contribution to severe convection: A case study example, Weather Forecast., 2, 3–16, 1987.

Fovell, R. G.: Convective initiation ahead of the sea-breeze front, Mon. Weather Rev., 133, 264–278, 2005.

Heiblum, R. H., Koren, I., and Altaratz, O.: Analyzing coastal precipitation using TRMM observations, Atmos. Chem. Phys., 11, 13201–13217, doi:10.5194/acp-11-13201-2011, 2011.

Horvath, K., Lin, Y.-L., and Ivančan-Picek, B.: Classification of Cyclone Tracks over Apennines and the Adriatic Sea, Mon. Weather Rev., 136, 2210–2227, 2008.

Hu, X. M., Nielsen-Gammon, J. W., and Zhang, F.: Evaluation of three Planetary boundary layer schemes in the WRF model, J. Appl. Meteorol. Clim., 49, 1831–1844, 2010.

Kingsmill, D. E.: Convection initiation associated with a sea breeze front, a gust front and their collision, Mon. Weather Rev., 123, 2913–2933, 1995.

Kolios, S. and Feidas, H.: A warm season climatology of mesoscale convective systems in the Mediterranean basin using satellite data, Theor. Appl. Climatol., 102, 29–42, 2010.

Manzato, A.: The 6 h climatology of thunderstorms and rainfalls in the Friuli Venezia Giulia Plain, Atmos. Res., 83, 336–348, 2007.

Manzato, A.: Hail in Norteast Italy: Climatology and bivariate analysis with the sounding-derived indices, J. Appl. Meteorol. Clim., 51, 449–467, 2012.

Mastrangelo, D., Horvath, K., Riccio, A., and Miglietta, M. M.: Mechanisms for convection development in a long-lasting heavy precipitation event over southeastern Italy, Atmos. Res., 100, 586–602, 2011.

Mazón, J. and Pino, D.: The role of sea-land air thermal difference, shape of the coastline and sea surface temperature in the nocturnal offshore convection, Tellus, 65A, 20027, doi:10.3402/tellusa.v65i0.20027, 2013.

Miao, J.-F., Wyser, K., Chen, D., and Ritchie, H.: Impacts of boundary layer turbulence and land surface process parameterizations on simulated sea breeze characteristics, Ann. Geophys., 27, 2303–2320, doi:10.5194/angeo-27-2303-2009, 2009.

Miglietta, M. M. and Rotunno R.: Numerical simulations of conditionally unstable flows over a mountain ridge, J. Atmos. Sci., 66, 1865–1885, 2009.

Mikuš, P., Prtenjak, M. T., and Strelec Mahović, N.: Analysis of the convective activity and its synoptic background over Croatia, Atmos. Res., 104/105, 139–153, 2012.

Miller, S. T. K., Keim, B. D., Talbot, R. W., and Mao, H.: Sea breeze: Structure, forecasting, and impacts, Rev. Geophys., 41, 1011, doi:10.1029/2003RG000124, 2003.

Nicholls, M. E., Pielke, R. A., and Cotton, W. R.: A two-dimensional numerical investigation of the interaction between sea breezes and deep convection over the Florida peninsula, Mon. Weather Rev., 119, 298–323, 1991.

Papanastasiou, D. K., Melas, D., and Lissaridis, I.: Study of wind field under sea breeze conditions; an application of WRF model, Atmos. Res., 98, 102–117, 2010.

Pozo, D., Borrajero, I., Marín, J. C., and Raga, G. B.: A numerical study of cell merger over Cuba – Part I: implementation of the ARPS/MM5 models, Ann. Geophys., 24, 2781–2792, doi:10.5194/angeo-24-2781-2006, 2006.

Prtenjak, M. T. and Grisogono, B.: Sea-land breeze climatological characteristics along the northern Croatian Adriatic coast, Theor. Appl. Climatol., 90, 201–215, 2007.

Prtenjak, M. T., Grisogono, B., and Nitis, T.: Shallow mesoscale flows at the north-eastern Adriatic coast, Q. J. Roy. Meteorol. Soc., 132, 2191–2216, 2006.

Prtenjak, M. T., Viher, M., and Jurković, J.: Sea-land breeze development during a summer bora event along the north-eastern Adriatic coast, Q. J. Roy. Meteorol. Soc., 136, 1554–1571, 2010.

Qian, J.-H.: Why Precipitation Is Mostly Concentrated over Islands in the Maritime Continent, J. Atmos. Sci., 65, 1428–1441, 2008.

Rakovec, J., Gabersek, S., and Vrhovec, T.: Relief shapes and precipitation on the south side of the Alps – Part I: Relief characteristics and dry sensitivity simulations, Meteorol. Z., 13, 83–90, 2004.

Saito, K., Keenan, T., Holland, G., and Puri, K.: Numerical simulation of the diurnal evolution of tropical island convection over the Maritime Continent, Mon. Weather Rev., 129, 378–400, 2001.

Shepherd, J. M., Ferrier, B. S., and Ray, P. S.: Rainfall Morphology in Florida Convergence Zones: A Numerical Study, Mon. Weather Rev., 129, 177–197, 2001.

Sherwood, S. C., Roca, R., Weckwerth, T. M., and Andronova, N. G.: Tropospheric water vapour, convection and climate, Rev. Geophys., 48, RG2001, doi:10.1029/2009RG000301, 2010.

Simpson, J. E.: Gravity currents in the environment and the laboratory, 2nd Edn., Cambridge University Press, UK, 1997.

Skamarock, W. C., Klemp, J. B., Dudhia, J., Gill, D. O., Barker, D. M., Duda, M. G., Huang, X.-Y., Wang, W., and Powers, J. G.: A description of the Advanced Research WRF version 3. NCAR/TN-4751STR, 113 pp., 2008.

Sow, K. H., Juneng, L., Tangang, F. T., Hussin, A. G., and Mahmud, M.: Numerical simulation of a severe late afternoon thunderstorm over Peninsular Malaysia, Atmos. Res., 99, 248–262, 2011.

Stechmann, S. N. and Majda, A. J.: Gravity Waves in Shear and Implications for Organized Convection, J. Atmos. Sci., 66, 2579–2599, 2009.

Strelec Mahović, N. and Zeiner, B.: Application of Meteosat SEVIRI channel difference 0.6 µm–1.6 µm in convective cells detection, Atmos. Res., 93, 270–276, 2009.

Ulanski, S. and Garstang, M.: The role of surface divergence and vorticity in the lifecycle of convective rainfall, Part I: Observation and analysis, J. Atmos. Sci., 35, 1047–1062, 1978.

Van Zomeren, J. and Van Delden, A.: Vertically integrated moisture flux convergence as a predictor of thunderstorms, Atmos. Res., 83, 435–445, 2007.

Van Delden, A.: The synoptic setting of thunderstorms in western Europe, Atmos. Res., 56, 89–110, 2001.

Wakimoto, R. M.: The life cycle of thunderstorm gust fronts as viewed with Doppler radar and rawinsonde data, Mon. Weather Rev., 110, 1060–1082, 1982.

Wang, D., Miao, J., and Tan, Z.: Impacts of topography and land cover change on thunderstorm over the Huangshan (Yellow Mountain) area of China, Nat. Hazards, 67, 675–699, 2013.

Weisman, M. L., Christopher, D., Wang, W., Manning, K. W., and Klemp, J. B.: Experiences with 0–36-h explicit convective forecasts with the WRF-ARW model, Weather Forecast., 23, 407–437, 2008.

Wilson, J. W. and Megenhardt, D. L.: Thunderstorm initiation, organization, and lifetime associated with Florida boundary layer convergence lines, Mon. Weather Rev., 125, 1507–1525, 1997.

Yuter, S. E. and Houze Jr., R. A.: Three-dimensional kinematic and microphysical evolution of Florida cumulonimbus. Part I: Spatial distribution of updrafts, downdrafts and precipitation, Mon. Weather Rev., 123, 1921–1940, 1995.

Žagar, N., Žagar, M., Cedilnik, J., Gregorič, G., and Rakovec, J.: Validation of mesoscale low-level winds obtained by dynamical downscaling of ERA40 over complex terrain, Tellus, 58A, 445–455, 2006.

Appendix A

Model verification by the near-surface measurements

Figure A1 shows the 24 h evolution of both the measured and modelled wind from the smallest domain above Pula airport site for all four examined cases. For all of them, the model reproduces the observed daily wind cycle with fairly good accuracy; particularly the SB onset, SB maximum and the SB fading (cases C1–C3 in Fig. A1). Diurnal wind variations in cases C1 and C3 clearly demonstrate the development of the undisturbed SB systems near the tip of the peninsula. The wind rotates from a night-time NE direction to the morning easterly and afternoon SW directions, thus describing all features observed in the SB/LB "climatology" for this station (Prtenjak and Grisogono, 2007). In case C2, the measured diurnal SB evolution was interrupted by the convective activity what was also satisfactorily recreated by the model. However, the model was less successful in forecasting the night-time calms and low wind speeds that are usually connected with significantly variable directions. The wind in this situation is difficult to measure accurately and to simulate correctly with the model. This type of model behaviour, which could arise due to the used parameterisations of the model and information about the complex terrain characteristics, has already been observed so far in a large number of modelling studies (e.g. Žagar et al., 2006; Borge et al., 2008; Challa et al., 2009; Papanastasiou et al., 2010).

To verify the model ability in the correct simulation of the chosen periods the statistics for selected cases (here for C1–C3) is also shown. The statistical evaluation is presented by a set of widely used statistical parameters (e.g. Borge et al., 2008) for the same station (Pula airport) in Table A1. A comparison was performed for the 2 m temperature (T; °C), humidity mixing ratio (q; g kg^{-1}) and relative humidity (rh; %) and the 10 m wind speed (WS; m s^{-1}) and wind direction (WD; deg). The set of statistical indices consisted of the mean value, bias, root mean square error (RMSE), mean absolute error (MAE) and the index of agreement (IOA). Because the focus was on the daytime Cb and SB interaction over the whole peninsula, the model ability to predict the mesoscale conditions was also estimated at 14:00 CET (called total in Table A1) using all available meteorological and climatological measurements (shown in Fig. 1).

The magnitudes of the statistical indices in Table A1 indicate a model overestimation in time and space regarding the near-surface wind speed. The best wind speed results (see total in Table A1) were obtained for case C3 followed closely by case C1. The best prediction of the near-surface wind direction (the smallest RMSE and MAE) can be noted for case C3 as well. In case C2, however, the model was less successful but still produced MAE values similar to those in, for example, Borge et al. (2008). The temperature is slightly but consistently under predicted (the most in case C3) with RMSEs in the range of 2.2–3.7. While the Pula airport station IOA values for temperature are very high (approximately 0.9, at 14:00 CET), the underestimations of the early afternoon temperature maxima over the peninsula are more pronounced. The same "colder" daytime condition was observed in sensitivity studies that examined the influence of the PBL scheme on the mesoscale thermodynamical characteristics (e.g. Weisman et al., 2008; Borge et al., 2008; Challa et al., 2009; Hu et al., 2010). Additionally, it was observed that the MYJ PBL scheme produces colder conditions than those measured, the humidity is usually overestimated (e.g. Hu et al., 2010). Although, similar conclusions can be drawn in selected cases, particularly case C1, where the modelled PBL is somewhat more humid than in reality, the low-level humidity prediction is very acceptable. The deviations from the measurements in rh are less (RMSE < 17.4) than those by Challa et al. (2009) (RMSE < 24) and are less for q than those by Borge et al. (2008) (IOA ϵ (0.41–0.53)). Despite these PBL scheme limitations, by considering the overall statistics and the additional sensitivity evaluation of the WRF model for the SB and Cb interaction, we have found that this model set-up and these modelled cases are acceptably simulated.

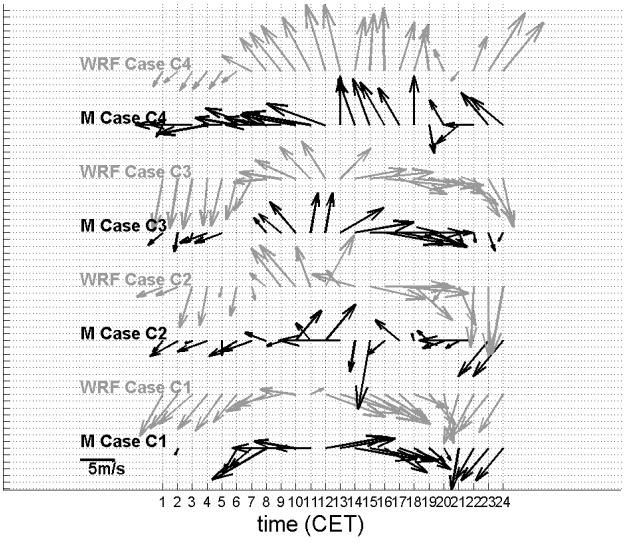

Fig. A1. Diurnal cycle of wind vectors provided by the measurements (M) from Pula airport site (black) and from the smallest WRF model domain (grey) for four selected cases (C1; 9 July 2006), (C2; 8 August 2006), (C3; 8 June 2003) and (C4; 7 July 2009) in Table 1.

Table A1. Some statistics for numerical simulations of cases C1 to C3 – mean measured and modelled values, BIAS, root mean square error (RMSE), mean absolute error (MAE), and the index of agreement (IOA). A comparison was done for 10 m wind speed (WS; $m\,s^{-1}$), wind direction (WD; deg), 2 m temperature (T; °C), humidity mixing ratio (q; $g\,kg^{-1}$) and relative humidity (rh; %). For Pula airport, statistical indices were calculated for the time series of wind and temperature for cases C1–C3. In the table, total represents spatial comparison between model data and data from stations in Fig. 1 at 14:00 CET in three chosen cases.

		Pula airport, 9 Jul 2006					Total, 14:00 CET			
	Statistic	WS ($m\,s^{-1}$)	WD (°)	T (°C)	q ($g\,kg^{-1}$)	rh (%)	WS ($m\,s^{-1}$)	WD (°)	T (°C)	rh (%)
case C1	$\overline{M}$	2.5		24.8	12.2	63.2	2.9		28.2	54.6
	$\overline{\mathrm{WRF}}$	3.8		24.1	14.1	73.8	3.8		27.1	59.8
	BIAS	1.3		−0.7	2.0	10.8	0.9		−1.1	5.2
	RMSE	1.2	37.2	2.6	2.1	17.4	1.5	64.3	3.4	15.3
	MAE	0.9	18.4	2.3	2.0	16.2	1.2	45.5	4.5	12.7
	IOA	0.8		0.9	0.6	0.6	0.7		0.7	0.6
		Pula airport, 8 Aug 2006					Total, 14:00 CET			
	Statistic	WS ($m\,s^{-1}$)	WD (°)	T (°C)	q ($g\,kg^{-1}$)	rh (%)	WS ($m\,s^{-1}$)	WD (°)	T (°C)	rh (%)
case C2	$\overline{M}$	2.0		22	12.3	74.2	3.3		25.7	57.4
	$\overline{\mathrm{WRF}}$	2.6		22.1	12.4	73.2	4.2		23.6	63.5
	BIAS	0.6		0.1	0.1	−1.0	0.9		−2.1	6.1
	RMSE	1.4	78.7	2.2	1.4	11.0	2.1	80.5	2.7	15.4
	MAE	1.2	65.7	1.8	1.2	8.8	1.8	62.5	1.9	12.6
	IOA	0.6		0.9	0.6	0.8	0.7		0.6	0.5
		Pula airport, 8 Jun 2003					Total, 14:00 CET			
	Statistic	WS ($m\,s^{-1}$)	WD (°)	T (°C)	q ($g\,kg^{-1}$)	rh (%)	WS ($m\,s^{-1}$)	WD (°)	T (°C)	rh (%)
case C3	$\overline{M}$	1.6		25	14.5	74.7	3.0		29.8	58.7
	$\overline{\mathrm{WRF}}$	2.9		23.9	14.5	76	2.9		26.8	68.5
	BIAS	1.3		−1.1	0	1.3	−0.1		−3.0	10.7
	RMSE	1.5	32.6	2.7	1.9	15.3	1.1	40.2	3.7	15.1
	MAE	1.3	26.0	2.5	1.5	13.2	0.9	32.6	3.3	12.6
	IOA	0.6		0.9	0.6	0.7	0.6		0.5	0.5